On the importance of phenology-water interactions in the evaporative process of the miombo woodland: Could it be why satellite-based evaporation estimates differ?

*Henry M. Zimba[1'2], Miriam Coenders-Gerrits[1], Kawawa E. Banda[3], Petra Hulsman[4], Nick van de Giesen[1], Imasiku A. Nyambe[3], Hubert. H. G. Savenije[1].

[1] Water Resources Section, Faculty of Civil Engineering and Geosciences, Delft University of Technology, Stevinweg 1, 2628 CN Delft, The Netherlands.

[2] Department of Agriculture, Ministry of Agriculture, P.O. Box 50595, Mulungushi House, Independence Avenue, Lusaka, Zambia.

[3] Integrated Water Resources Management Centre, Department of Geology, School of Mines, University of Zambia, Great East Road Campus, Lusaka, Zambia.

[4] Ghent University, Hydro-Climate Extremes Lab (H-CEL), Coupure links 653, 9000 Ghent, Belgium

*Corresponding author: a.m.j.coenders@tudelft.nl

Abstract

The miombo woodland is the largest dry woodland formation in sub-Sahara Africa with a spatial extent approximated between $2.7 – 3.6$ million km^2. In comparison to other global ecosystems the miombo woodland exhibits unique phenology-water interactions such as increase in the leaf area index (LAI) with access to deep soil moisture in the dry season. However, due to limited flux observations in the miombo region, there is scarcity of information on the influence of these phenology-water interactions on the evaporation of the miombo woodland, and it is also not known if these interactions are accurately represented in satellite-based evaporation estimates. Enhancing the accuracy of hydrological and climate modelling for the miombo region requires deepened understanding and appropriately representing the phenology-water interactions in the simulations. Therefore, in this study trends and magnitudes of six satellite-based evaporation estimates; FLEXI-Topo, GLEAM, MOD16, SSEBop, TerraClimate and WaPOR, are compared across the different canopy phenophases of the miombo woodland in a representative river basin, Luangwa Basin, in southern Africa. We observe if the trends and magnitudes of the satellite-based evaporation estimates aligns with the documented phenology-water interactions of the miombo woodland. In the absence of basin scale field observations, the actual evaporation estimated using the general annual water balance is used, where the water balance inferred actual evaporation (E_{wb}) is equal to precipitation minus discharge for long-term averages. The six satellite-based evaporation estimates are compared to E_{wb} in order to observe whether they underestimate or overestimate evaporation in a predominantly miombo woodland river basin. Results show substantial coefficients of variations ($28 – 58$ %) among satellite-based evaporation estimates in the cool-dry season, warm dry season and warm-pre-rainy season (dormant and green-up phenophases) when the miombo species undergoes substantial changes in the canopy phenology such as the simultaneous leaf fall and leaf flush and accesses to deeper soils moisture to buffer dry season conditions. Most low correlation coefficients ($r < 0.5$) among satellite-based evaporation estimates are also observed in the dormant phenophase in the dry season. The lowest coefficients of variations ($7- 11$%) in magnitudes of satellite-based evaporation estimates are observed in the rainy season with high temperature, high leaf chlorophyll content and highest LAI in the maturity/peak phenophase(s).

Compared to the basin scale annual water balance actual evaporation, all six satellite-based evaporation estimates appear to underestimate evaporation at basin scale. While the Luangwa Basin is not entirely covered with the miombo woodland, as it is composed of other woodland types as well, such as the mopane woodland, the observed underestimation shows the general performance of the satellite-based evaporation estimates. Overall, it appears the inadequate understanding and inaccurately representing of the phenology-water interactions of the miombo species in evaporation simulations possibly result in the observed differences in satellite-based evaporation estimates. Based on this study field-based observations of the evaporation of the different canopy phenophases and strata of the miombo woodland are needed and to compare with satellite-based evaporation estimates.

1   Introduction

"Vegetation phenology" refers to the periodic biological life cycle events of plants, such as leaf flushing and senescence, and corresponding temporal changes in vegetation canopy cover (Stökli *et al.,* 2011; Cleland *et al.*, 2007). Plant phenology and climate are highly correlated (Pereira *et al.,* 2022; Niu *et al.*, 2013; Cleland *et al.,* 2007). Plant phenological responses to trigger elements, such as temperature, hydrological and day light regimes, include among others leaf fall and leaf flush, budburst, flowering and variation in photosynthetic activity due to changes in chlorophyll levels (Pereira *et al.,* 2022; Niu *et al.*, 2013; Cleland *et al.,* 2007). The phenological responses are species-dependent and are controlled by adapted physiological properties (i.e., Lu *et al*., 2006). Plant phenology controls the access to critical soil resources such as nutrients and water (Nord and Lynch, 2009). The phenological response influences plant canopy cover and affects plant-water interactions. For instance, the phenophases associated variations in canopy leaf display, i.e., due to leaf fall and leaf flush, influences how much radiation is intercepted by plants (Shahidan, Salleh, and Mustafa, 2007). Intercepted radiation influences canopy conductance. In water limited conditions, at both individual species and woodland scales, leaf fall reduces canopy radiation interception while leaf flush and the consequent increase in canopy cover increases canopy radiation interception leading to increased transpiration (Snyder and Spano, 2013) controlled by available moisture storage, both vegetative and root zone. Plant canopy cover and its interactions with atmosphere carbon dioxide through the photosynthetic and autotrophic respiration processes influences transpiration. Ultimately, plant phenological response to changes in the trigger elements influences transpiration and actual evaporation of the woodland (i.e., Marchesini *et al.,* 2015).

Evaporation of woodland surfaces accounts for a significant portion of the water cycle over the terrestrial land mass (Sheil, 2018; Van Der Ent *et al*., 2014; Gerrits, 2010; Van Der Ent *et al*., 2010). Miralles *et al.* (2020) defined evaporation as "the phenomenon by which a substance is converted from its liquid into its vapour phase, independently of where it lies in nature". In this study we adopt the term evaporation for all forms of terrestrial evaporation, including transpiration by leaves, evaporation from intercepted rainfall by vegetation and woodland floor, soil evaporation, and evaporation from stagnant open water and pools (Miralles *et al.,* 2020; Savenije, 2004). Understanding the characteristics of evaporation, such as interception and transpiration, in various woodland ecosystems is key to monitoring the climate impact on woodland ecosystems, for hydrological modelling and the management of water resources at various scales (Kleine *et al.,* 2021; Bonnesoeur *et al.,* 2019; Roberts, (undated)). One of the key aspects to enable this

understanding is the knowledge of the woodland phenology interactions with climate variables and seasonal environmental regimes (i.e., Zhao *et al.,* 2013). Environmental variables such as precipitation and temperature influences plant phenology differently across the diverse ecosystems globally (Forrest *et al.,* 2010; Forrest & Miller-Rushing, 2010; Kramer *et al.,* 2000). Additionally, Tian *et al.* (2018) showed that various water cycle components in several ecosystems globally indicates that plants have adapted to local and regional climatic conditions such as variations in precipitation, temperature, active photosynthetic radiation and abiotic conditions such as soil type and soil water supply at the ecosystem scale. The findings by Tian *et al.* (2018) are "evidence of global differences in the interaction between plant water storage and leaf phenology". Therefore, understanding the plant phenology-water interactions at local and regional scales with minimal variations and appropriately incoporating these aspects in hydrological and climate modelling is likely to improve accuracy of the simulations (i.e., Forster *et al*., 2022).

The miombo woodlands is the largest dry woodland formation in sub-Sahara Africa with a spatial extent approximated between $2.7 - 3.6$ million km^2 (Ryan *et al.*, 2016; Frost, 1996; White, 1983). Despite their significance in biodiversity (Mittermeier *et al.,* 2003, White, 1983), carbon sink (Pelletier *et al.,* 2018) and their role in the food, energy and water nexus (Beilfuss, 2012; Campbell *et al.,* 1996; Frost, 1996) the miombo woodlands have received little attention in terms of understanding of the evaporation in relation to the phenology of woodlands. The uniqueness, compared to other global ecosystems, of the plant-water interactions of the miombo woodland has been highlighted (Tian *et al.,* 2018; Guan *et al.,* 2014; White, 1983), and has been particularly demonstrated by Tian *et al.* (2018) Vinya *et al.,* (2018), Fuller (1999), Frost (1996) and White (1983). Of importance are the adapted endogenous whole-plant control of leaf phenology (i.e., Vinya *et al.,* 2018), simultaneous leaf fall (leaf shedding) and leaf flush (i.e., Fuller, 1999) and deep rooting which gives ability to the miombo species to access deep soil moisture, including groundwater resources, to buffer the dry season water limitations (Tian *et al.,* 2018; Guan *et al.,* 2014, Savory, 1963). Furthermore, the new canopy biomass formation in form of new leaf flushing occurs before the commencement of seasonal rainfall (Chidumayo, 1994; Fuller and Prince, 1996). The new young flushed leaves in the dry season have high water content of up to 66% which declines to about 51% as the leaves harden until they are shed off in the next season (Ernst and Walker, 1973). The miombo woodland is heterogeneous with diverse plant species whose phenological response to stimuli is characteristically species dependent (Chidumayo, 2001; Fuller, 1999; Frost, 1996). For instance, leaf fall, leaf flush and leaf colour change are triggered at different times for each species. This means that for the miombo woodland, unlike ~~what obtains~~ in other homogenous woodlands in which the entire woodland is either undergoing leaf fall or leaf flush, the leaf fall and leaf flush occur simultaneously. The simultaneous leaf fall and leaf flush results in a woodland canopy that is variable in terms of canopy closure and greenness especially during the dry season. To this effect the miombo woodland has varied canopy closure ranging between 2 to about 70 percent depending on the miombo woodland strata and local environmental conditions such as rainfall, soil type, soil moisture, species composition and temperature (Chidumayo, 2001; Fuller, 1999; Frost, 1996). For the wet miombo woodland with a canopy closure of about 70 percent, at any given time, there is a relatively large woodland canopy surface for radiation/energy interception. The deep rooting in most miombo species (Savory, 1963) provides access to deep soil moisture resources (Fan *et al.,* 2017; Kleidon and Heimann, 1998). The deep rooting miombo species green canopy provides an evaporative surface that, in combination with other environmental variables, possibly facilitates continued transpiration even during the driest periods within moisture stress threshold (i.e., Li *et al.,* 2021). Most miombo species are broad leaved with

capacity for radiation interception (Fuller, 1999) and rainfall interception of up to 20% in wet miombo woodland (Alexandre, 1977). In the miombo woodland soil moisture increases with depth (Chidumayo, 1994; Jeffers and Boaler, 1996; Savory, 1963). These adapted miombo species phenological and physiological attributes influences the evaporative processes (Forster *et al*., 2022; Snyder *et al*., 2013; Schwartz, 2013). The question is whether actual field evaporation reflects these interactions between phenology, environmental variables and the adapted physiological attributes of miombo species. Additionally, do satellite-based evaporation estimates adequately represent the various phenological transitions and account for these unique miombo species dry season phenology (i.e., changes in canopy cover) –water interactions within the available energy and soil moisture storage dynamics at play? Regardless the above highlighted uniqueness and importance of the miombo woodland, there exists scant, if any, information on the woodland evaporation dynamics. This is due to lack of flux observation towers in the entire miombo woodland. Furthermore, most of the studies conducted in the miombo woodland have tended towards the characterisation of woodland plant species, its role as a carbon sink and the social-economic relevance of the ecosystem. Information on the phenology of the miombo woodland plants exists (i.e., Chidumayo *et al.,* 2010; Chidumayo, 2001; Fuller, 1999; Chidumayo and Frost, 1996) but there has been extremely limited attempts to characterise evaporation trends and magnitudes linking them to the phenology-water interactions of the ecosystem with access to ground water resources, especially during the water scarce dry season. For instance, the only (based on information in public domain) point-based field observations of evaporation of the wet miombo woodland by Zimba *et al.* (2013) are not sufficient to make any definitive conclusions about the evaporative dynamics of this vast ecosystem.

In the absence spatially distributed field observations of evaporation satellite-based evaporation estimates are seen as a valuable alternative though they come with their own limitations (Zhang *et al.,* 2016). For instance, evaporation is land cover dependent i.e., evaporation from an open water body, woodland and grassland (Han et *al.,* 2019; Liu & Hu*,* 2019; Wang *et al.,* 2012). However, because of the differences in algorithms, process and inputs the satellite-based evaporation estimates differ for the same land surface (i.e., woodland) (Zhang *et al.,* 2016; Cheng *et al.,* 2014). Currently, satellite-based evaporation estimates at various scales are available (i.e., Global land evaporation Amsterdam model (GLEAM) (Martens et al., 2017; Miralles et al., 2011); Moderate-resolution imaging spectrometer (MODIS) MOD16) (Running et al., 2019; Mu et al., 2011; Mu et al., 2007); Operational simplified surface energy balance (SSEBop) (Senay et al., 2013); and Water productivity through open access of remotely sensed derived data (WaPOR) (FAO, 2018)). Classification of the various satellite-based evaporation estimates have been extensively discussed by Zhang *et al.* (2016), Jiménez *et al.* (2011) and Jiménez, Prigent & Aires (2009). These satellite-based evaporation estimates are mainly designed to assess evaporation of agricultural crops (i.e., Biggs *et al.,* 2015; Zhang *et al.,* 2016). However, natural woodlands have different adapted phenology-water interactions and evaporation (Wang-Erlandsson *et al.*, 2016; Snyder and Spano, 2013; Schwartz, 2013). There is currently no publication in the public domain showing how various satellite-based evaporation estimates compare in the miombo woodland, especially with a focus on the miombo species phenological-physiological interactions across different phenophases and seasons. Yet, the usage of satellite-based evaporation estimates in hydrological modelling, climate modelling and the management of water resources globally and in Africa is on the increase (i.e., García *et al.*, 2016; Zhang *et al., 2016;* Makapela, 2015). However, because of the absence or scarce field observations and extremely limited validation, it is impossible to know which satellite-based evaporation estimates are close to actual physical

180 conditions of the miombo woodland. In most cases, the choice for a satellite-based evaporation product is based on validation results in non-miombo woodlands or at a scale (i.e., Weerasinghe *et al.*, 2020) that includes other woodland types. This product choice scenario is a challenge in that non-miombo woodlands have a different phenology and evaporation to that of the miombo ecosystem. For instance, an evaporation estimation approach that performs extremely well in

185 energy limited conditions and homogeneous woodlands, e.g., in Europe, (i.e., Bogawski and Bednorz, 2014) cannot be assumed to have the same performance in a warm, water limiting and heterogeneous woodland such as the miombo. Although, Weerasinghe *et al.* (2020) compared satellite-based evaporation estimates in the Zambezi Basin, whose vegetation cover, among many others, comprise the miombo woodland, the focus of their study was not on the miombo woodland.

190 Furthermore, Weerasinghe *et al.* (2020) did not attempt to link the differences in the satellite-based evaporation estimates to the phenology of the miombo woodland. The results they observed at the Zambezi Basin scale might be different at sub-basin level such as the Luangwa Basin, and in the miombo woodland.

Therefore, this study was formulated in order to contribute to the bridging of the gap in

195 information on satellite-based evaporation estimates performance in different phenophases of the miombo woodland. We focused on the Luangwa sub-basin in the larger Zambezi Basin, one of the largest river basins in the miombo ecosystem. The Luangwa Basin was chosen because it is situated in a sparsely gauged region (Beilfuss, 2012), where it is essential that management of water resources is based on reliable information, for various competing uses, i.e. hydropower,

200 agriculture, wildlife, industrial and domestic (WARMA, 2022). The Luangwa Basin is located in both dry (i.e., southern miombo woodlands) and wet (i.e., central Zambezian miombo woodlands) miombo. The central Zambezian miombo woodland is the largest of the four miombo woodland sub-groups, the other three being the Angolan miombo woodland, eastern miombo woodland, and the southern miombo woodland (Frost, 1996; White, 1983). The Luangwa Basin is also located in

205 Zambia, argued to have the highest diversity of miombo woodland trees and considered centre of endemism for the miombo woodlands Brachystegia species (Frost, 1996). The largest area of the Luangwa Basin is covered by the miombo woodland with the mopane woodland occupying by far a smaller area of the basin (Frost, 1996; White, 1983). These attributes suggest a catchment that provides a fair representation of the miombo woodlands conditions and an appropriate site for this

210 type of study.

Therefore, the aim of this study was two-fold:

(i) Compare the temporal trends and magnitudes of six freely available satellite-based evaporation estimates across different phenophases of the miombo woodland.

(ii) Compare satellite-based evaporation estimates to the water balance-based actual

215 evaporation estimates for the Luangwa Basin.

2 Materials and Methods
2.1 Study site

The location and extent of the miombo woodland in Africa is given in Fig. 1(a) (Ryan *et*

220 *al.*, 2016; White, 1983). The Luangwa (Fig. 1b) is a sub-basin in the larger Zambezi Basin in sub-Saharan Africa in Zambia with spatial extent of about 159,000 km^2 (Beilfuss, 2012; World Bank, 2010). Based on the miombo woodland delineation by White (1983) and Ryan *et al.* (2016) as given in Fig.1 (c) about 75 percent of the total Luangwa Basin land-mass is covered by the miombo woodland, both dry and wet miombo.

225
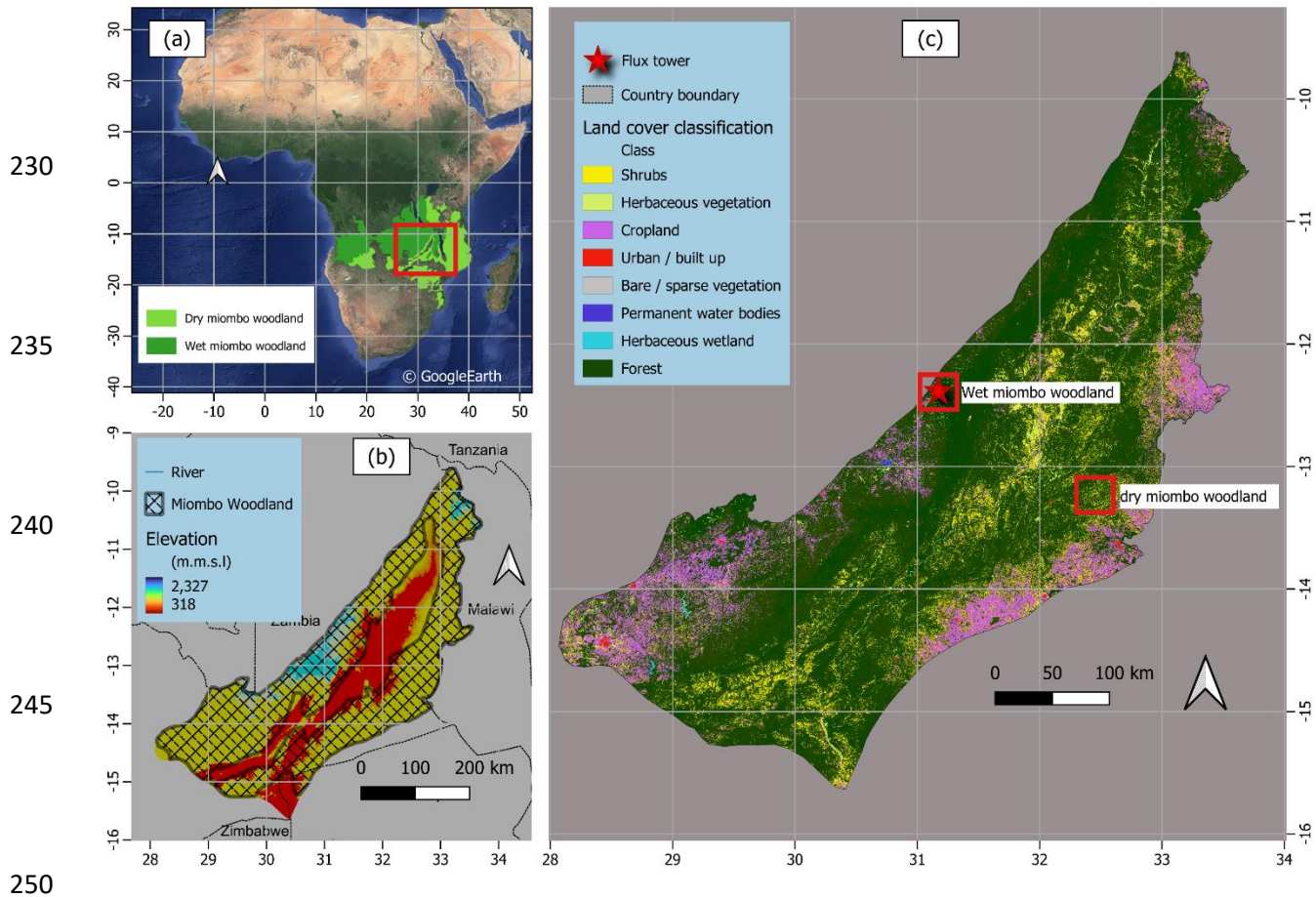
Figure 1: (a) Spatial extent of the miombo woodland in Africa and the location of the Luangwa Basin in Zambia. (b) Spatial distribution of elevation ASTER digital elevation model (DEM) and the extent ~~of~~ the miombo woodland in the Luangwa Basin. (c) Land cover characterisation of the Luangwa Basin based on the Copernicus land cover classification.

Additionally, statistics from the 2019 Copernicus land cover classification (Fig. A1 in the supplementary data), with 80 percent user accuracy and woodland classification accuracy of about 75% (Buchhorn *et al.,* 2020; Martins *et al.,* 2020), indicates that 77 percent of the total basin area is woodland (dense and open woodland) which is largely miombo woodland with a relatively smaller component of mopane woodland in the middle area of the basin (i.e., Fig. 1). Elevation (Fig. 1b) ranges between 329 – 2210 m above mean sea level with the central part generally a valley. The miombo woodland, both dry miombo woodland and wet miombo woodland, is generally in the upland (Fig.1b). The Luangwa River, 770 km long, and its tributaries drain the basin (Beilfuss, 2012). The Luangwa Basin is scarcely gauged (Beilfuss, 2012). This has resulted in a paucity of data on various hydrological aspects such as rainfall and discharge. The basin is located in a climate environment characterised by a well-delineated wet season, from October to April and a dry season, May to October. Furthermore, the dry season is split into the cool-dry (May to August) and hot dry (August to October) seasons. The movements of the inter-tropical convergence zone (ITCZ) over Zambia between October and April dominate the rainfall activity in the basin. The basin has a mean annual precipitation of about 970 mm yr^{-1}, potential evaporation of about 1560 mm yr^{-1}, and river runoff reaches about 100 mm yr^{-1} (Beilfuss, 2012; World Bank,

2010). The key character of the miombo woodland species is that they shed off old leaves and acquire new ones during the period May to October in the dry season. Depending on the amounts of rainfall received in the preceding rain season the leaf fall and leaf flush processes may start early (i.e., in case of low rainfall received) or late (in case of high rainfall received) and may continue up to November (i.e., in the case of high rainfall received) (Frost,1996).

2.2   Study approach

Firstly, the study sought to find out the extent to which satellite-based evaporation estimates agree with/differ from each other within the different canopy phenophases of the miombo woodland. The trends and magnitudes of satellite-based evaporation estimates across the different phenophases of the miombo woodland were compared. The comparison of the satellite-based evaporation estimates was conducted at pixel scale and at the Luangwa Basin miombo woodland scale. The comparison of satellite-based estimates was performed in order to observe if their trends and magnitudes were in tandem with the phenology-water interactions of the miombo species across different phenological seasons.

Secondly, point scale observations in the wet miombo woodland (Zimba *et al.*, 2023) showed that satellite-based evaporation estimates underestimated actual evaporation of the wet miombo woodland in phenophases in the dry season and early rainy season in the Luangwa Basin. However, the Luangwa Basin has a heterogenous land cover which includes mopane woodland and grasslands. The question was whether the heterogeneity in the land cover of the Luangwa Basin would result in satellite-based evaporation estimates performing contrary to the point-scale observations at a wet miombo woodland site when compared to the water balance-based evaporation estimates at basin scale.

For this study, a 12-year period, 2009 – 2020, was used for the assessments because satellite-based evaporation estimates were available for free for this period. The period also had cycles of low and high annual rainfall sufficient to show performance of satellite-based evaporation estimates under changing monthly and annual conditions.

The proceeding sections elaborates the methods used in this study.

2.2.1 Phenophases of the miombo woodland and assessment of phenological conditions

To categorise the phenophases two approaches were used; satellite-based classification and the climate and soil moisture classifications.

For this study satellite-based classification of phenophases was based on the National Aeronautics and Space Administration (NASA) Collection 6 MODIS Land Cover Dynamics (MCD12Q2) Product accessed from the https://modis.ornl.gov/globalsubset/, last access: 20 February, 2023 (Gray *et al.*, 2019; Friedl et *al.,* 2019; Zhang *et al.,* 2003). The MCD12Q2 uses the changes in canopy greenness to characterise the canopy phenophases (Friedl et *al.,* 2019; Gray *et al.,* 2019). For the miombo woodland in the Luangwa Basin eight phenophases were identified using the satellite-based data MCD12Q2 (Fig. 2). The satellite-based phenophases include: green-up, mid-green up, maturity, peak, senescence, green-down, and mid-green down and dormant. For easy of analysis the phenophases were merged into four groups based on dominant activity in each phenophase (Fig. 2). To compliment the MCD12Q2 classification the MODIS-based leaf area index (LAI) obtained from https://app.climateengine.org/climateEngine, last access: 20 February, 2023) (Myneni, Knyazikhin & Park, 2021; ORNL DAAC, 2018; Myneni & Park, 2015) and the normalised difference vegetation index (NDVI) (ORNL DAAC, 2018; Vermote and Wolfe, 2015) were used.

320

325

330

335

20 October, 2021   20 January, 2021   20 August, 2021   20 September, 2021
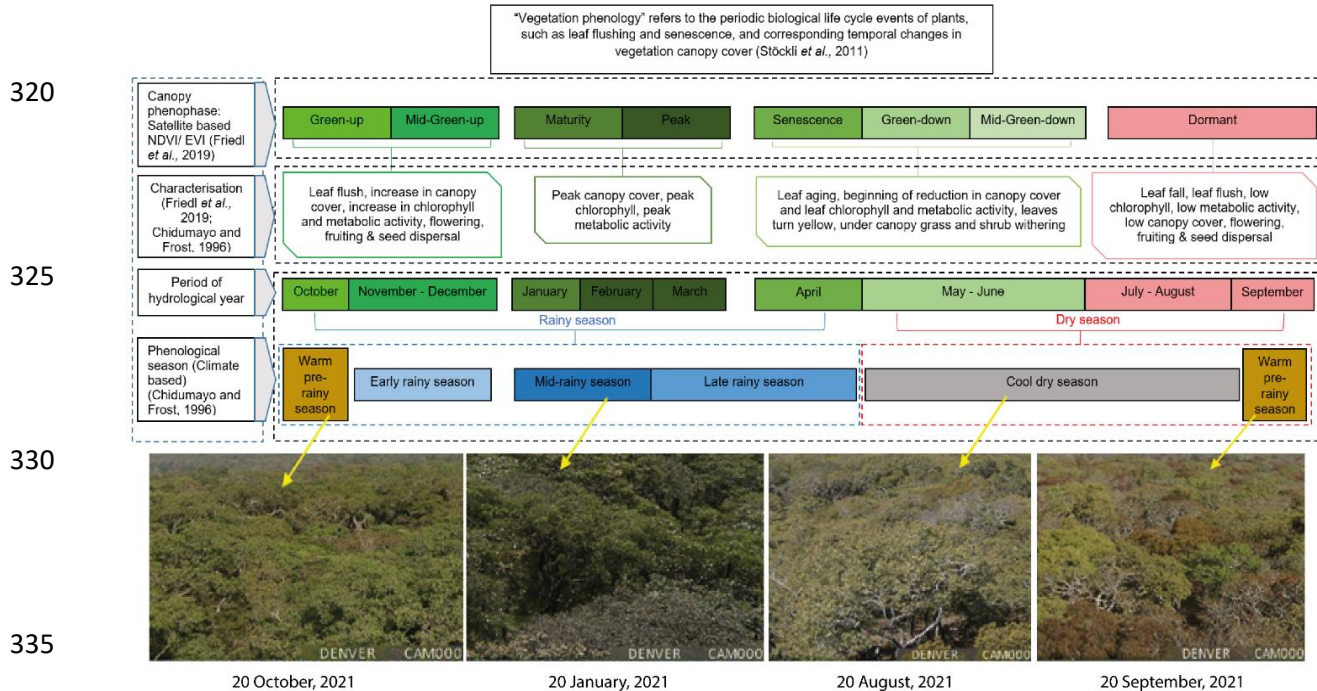
Figure 2: Characterisation of canopy phenophases of the miombo woodland in relation to seasonality for the Luangwa Basin. Photographs show the changes in the canopy cover on selected days across different phenophases of a wet miombo woodland for the year 2021.

340

The Satellite-based LAI and NDVI have been used as proxies to observe phenological conditions such as the canopy biomass formation, changes in the canopy closure (i.e., through leaf fall and leaf flush) and changes in canopy chlorophyll conditions (i.e., Guan *et al.,* 2014; Santin-Janin *et al*., 2009; Chidumayo, 2001; Fuller, 1999). Therefore, in this study the satellite-based LAI and NDVI were used as proxy for observing changes in phenological conditions of the miombo woodland across different phenological seasons. For the LAI the NASA's MCD15A3H product (Myneni, Knyazikhin & Park, 2021; ORNL DAAC, 2018; Myneni & Park, 2015) with a four-day temporal resolution and 500 m spatial resolution was used. The MODIS MOD09GQ.006 (Vermote and Wolfe, 2015) surface reflectance bands 1,5 and 6 were used to estimate the NDVI at daily temporal resolution and 250 m spatial resolution using the band ratio method. The daily NDVI values were then averaged into four-day values in order to have the same temporal resolution as the LAI.

For the climate and soil moisture-based classification Chidumayo and Frost (1996) observed five phenological seasons: warm pre-rainy season, early rainy season, mid-rainy season, late rainy season and the cool dry season (Fig. 2). Within these phenological seasons the phenology of miombo species transition through various stages i.e., from leaf fall/leaf flush, growth of stems, flowering to mortality of seed (Chidumayo and Frost,1996). The satellite-based phenophases can be identified within the climate-based phenological seasons (Fig. 2).

To compliment the observations in the satellite-based LAI and NDVI photographs from a digital camera (Denver WCT-8010) installed on the flux tower at a wet miombo woodland site in Mpika (Zimba *et al.,* 2023) were used to observe the changes in the canopy phenology of the miombo woodland across different phenophases from January to December in the year 2021 (see Fig. 7 in section 3.2). In addition, the fish-eye (LIEQI LQ-001) was used to obtain under-canopy

images. The images from under the canopy helped to observe the changes and differences in canopy leaf display (i.e., leaf fall, leaf flush and leaf colour changes) among miombo species.

2.2.2 Delineation of the miombo woodland areas used in this study

The comparison of satellite-based evaporation estimates was performed at two levels: pixel level at known dry miombo woodland and wet miombo woodland locations, and at entire miombo woodland scale in the Luangwa Basin (Figs. 1 and 3).
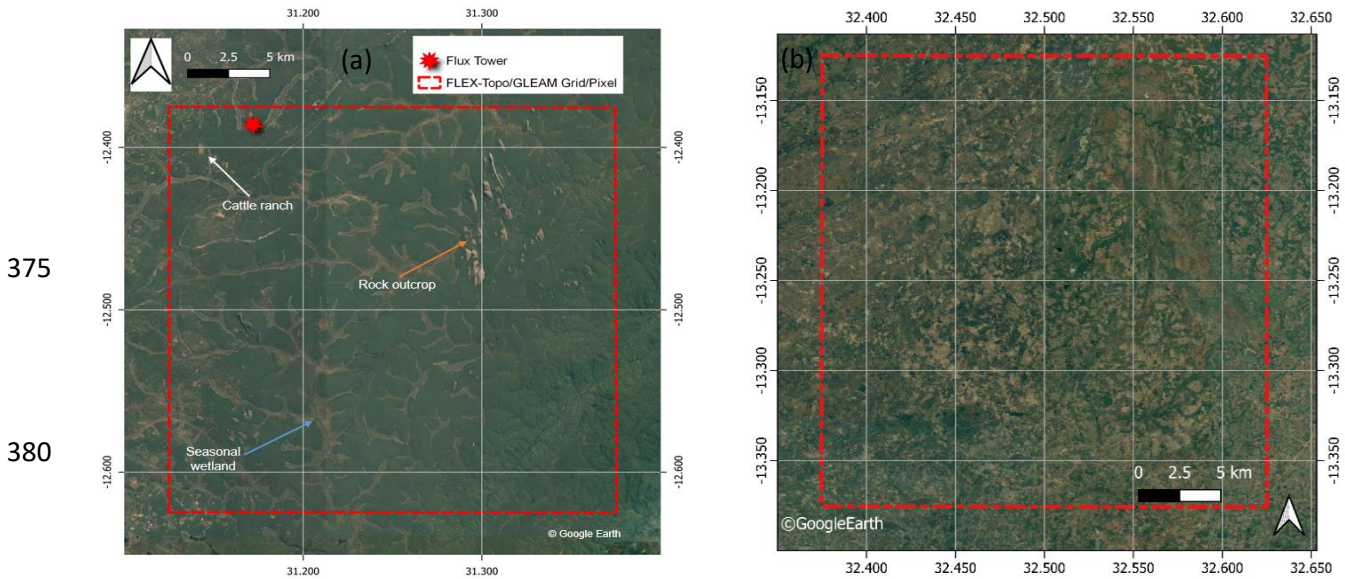
Figure 3: The wet miombo woodland (a) and dry miombo woodland (b) locations used for comparison of satellite-based evaporation estimates at FLEX-Topo and GLEAM spatial resolution (approximately 27.7 km by 27.7 km). The dotted red line is the actual location of the FLEX-Topo and GLEAM pixels.

Firstly, a pixel-based comparison was performed by using known undisturbed wet miombo woodland and dry miombo woodland locations (Figs. 1 and 3). The focus on a known wet miombo woodland enabled comparison of the field observations of the changes in canopy cover using digital camera images to the satellite-based LAI and NDVI for the year 2021. The pixel-based comparison used actual location of FLEX-Topo and GLEAM pixels with original spatial resolutions (approximately 27.7 by 27.7 km) (Fig. 3). For MOD16, SSEBop, TerraClimate and WaPOR, the mean of actual evaporation estimates in all the pixels within the dotted red square (Fig. 3) were used. See Section 2.2.3 and Table 1 for satellite-based evaporation estimates used in this study.

Secondly, the typical miombo woodland regions as categorised by White (1983) and Ryan *et al.* (2016) (see Fig. 1 a,b) were used to delineate the area covered by the miombo woodland in the Luangwa Basin. The delineated miombo woodland in the Luangwa Basin excluded the mopane woodland, mixed woodland as well as the large water bodies like dams. This delineation (as shown in Fig. 1) ensured that only the areas classified as typical miombo woodland (Ryan *et al.*, 2016; White, 1983) were considered in the analysis.

[handwritten note: ↑ how was this considered in the analysis?]

2.2.3 Satellite-based products used in the study

Compared to other ecosystems, Pelletier *et al.* (2018) and Tian *et al.* (2018) observed that the miombo woodland exhibit distinct behaviour (i.e., canopy display and the vegetation water content) during the dry season. To this effect this study compared the trends and magnitudes of six satellite-based evaporation estimates across the different phenophases of the miombo woodland with emphasis on the dry season. This was conducted in order to observe existence of discrepancies in monthly temporal trends and magnitudes of satellite-based evaporation estimates under changing phenological seasons. The six satellite-based evaporation estimates consisted of: 1) FLEX-Topo (Hulsman *et al.,* 2021; Hulsman *et al.,* 2020; Savenije, 2010); 2) Thornthwaite-Mather climatic water balance model (TerraClimate) (Abatzoglou *et al.,* 2018); 3) Global land evaporation Amsterdam model (GLEAM) (Martens *et al.,* 2017; Miralles *et al.,* 2011); 4) Moderate-resolution imaging spectrometer (MODIS) MOD16 (Running *et al.,* 2019; Mu *et al.,* 2011; Mu *et al.,* 2007); 5) Operational simplified surface energy balance (SSEBop) (Senay *et al.,* 2013) and 6) Water productivity through open access of remotely sensed derived data (WaPOR) (FAO, 2018). These satellite-based evaporation estimates were selected purely because they are free of charge and easily accessible from various platforms, and have an archive of historical data with the temporal and spatial resolutions suitable for use in this study. Except for FLEX-Topo and GLEAM (with spatial resolution of 27.7 km), these satellite-based evaporation estimates have relatively fine spatial resolution (i.e., 500 m, 1000 m, 4000 m and 250 m for MOD16, SSEBop, TerraClimate and WaPOR respectively) and temporal resolution (daily, 8-day, 10-day and monthly respectively), which attributes were suitable for this study. The original spatial resolutions were used because these satellite-based evaporation estimates are normally used as is, in their original resolutions. Resampling the different spatial resolutions of the satellite-based evaporation estimates to a single (uniform) spatial resolution was thought to be problematic as it would have introduced unknown and unquantifiable errors, regardless the extent resampled. For detailed explanations on the model structure, processes and inputs for the satellite-based evaporation estimates used in this study the reader is advised to refer to the cited literature above and in Table 1.

Other satellite-based products used in this study include the ASTER digital elevation model (DEM), MODIS-based LAI and NDVI, Copernicus land cover map, net radiation, precipitation, runoff, soil moisture and relative humidity. For detailed information (i.e., structure, processes and inputs) on the other satellite-based products used in this study the reader is advised to refer to the cited literature in Table 1.

2.2.4 Basin water balance–based actual evaporation

In cases where spatially distributed field measurements are not available, as is the case with large basins and more importantly in the Luangwa Basin, the use of the water balance approach using spatially distributed satellite-data is an acceptable approach (i.e., Weerasinghe *et al.,* 2020; Liu *et al.*, 2016). In this study the general annual water balance was conducted in order to have a general outlook on the performance of the satellite-based evaporation estimates at basin level.

Table 1. Characteristics of products used in the study

Variable	Product name	Time Period	Spatial coverage/Location	Temporal resolution	Spatial resolution	Reference	Source of data
Precipitation	CFSR v2	2009 - 2020	Global	Daily	19.2 km	(Saha et al., 2014; Saha et al., 2010)	Climate Engine portal
	CHIRPS	2009 - 2020	Global	Daily	4.8 km	(Funk et al., 2015)	Climate Engine portal https://app.climateengine.com/climateEngine
	ERA5	2009 - 2020	Global	Daily	24	(Hersbach et al., 2017)	Climate Engine portal
	TerraClimate	2009 - 2020	Global	Monthly	4 km	(Abatzoglou et al., 2018)	Climate Engine portal
Air temperature (mean)	CFSR v2	2009 - 2020	Global	Daily	19.2 km	(Saha et al., 2014; Saha et al., 2010)	Climate Engine portal
LAI	MODIS MCD15A3H v6	2021	Global	4-Day	0.5 km	(Myneni, Knyazikhin & Park, 2015)	Climate Engine portal
NDVI	MODIS MOD09GA v6	2021	Global	Daily	0.5 km	(Vermote & Wolfe, 2015)	Climate Engine portal
Runoff	Observations	1960-1992	159,000 km²	Daily	N/A		WARMA, Zambia
	TerraClimate	1960 - 2020	Global	Monthly	4 km	(Abatzoglou et al., 2018)	Climate Engine portal
Net radiation	CFSR v2	2009-2020	Global	Daily	19.2 km	(Saha et al., 2014; Saha et al. 2010)	Climate Engine portal
Soil moisture (25 cm)	CFSR v2	2009 - 2020	Global	Daily	19.2 km	(Saha et al., 2014; Saha et al. 2010)	Climate Engine portal
Relative humidity	CFSR v2	2009 - 2020	Global	Daily	19.2 km	(Saha et al., 2014; Saha et al., 2010)	Climate Engine portal
Elevation	ASTER GDEM v3	N/A	Global	N/A	30m	(Abrams and Crippen, 2019)	NASA Glovis portal
Land cover map	Copernicus CGLS-LC100 v3	2019	Global	Annual	100m	(Buchhorn et al., 2020)	Google Earth Engine
Actual evaporation	FLEX-Topo	2009 - 2020	Catchment	Daily	27.7 km	(Hulsman et al., 2021; Hulsman et al., 2020; Savenije, 2010)	ZAMSECUR Project – Delft Technical University
	GLEAM (v3.2a)	2009 -2020	Global	Daily	27.7 km	(Martens et al., 2017; Miralles et al., 2011)	GLEAM FTP server
	MOD16v2	2009 -2020	Global	8-Day	0.5 km	(Running et al., 2019; Mu et al., 2011)	Climate Engine portal: Global subsets tool: MODIS/VIIRS Land Products
	SSEBop	2009 -2020	Global	Monthly	1 km	(Senay et al., 2013).	Climate Engine portal
	TerraClimate	2009 -2020	Global	Monthly	4 km	(Abatzoglou et al., 2018)	Climate Engine portal
	WaPOR v2, (ETLook)	2009 -2020	Continental	10-Day	0.25 km	(FAO, 2018)	WaPOR Portal

455

460

465

470

475

480

485

490

495

The general basin annual average water balance-based evaporation ($E_{a(wb)}$) is estimated using Eq. (1) where long-term over-year storage change is neglected.

500     $$E_{a(wb)} = P - Q \tag{1}$$

where, P is the annual average catchment precipitation in mm year^{-1} and Q is annual average discharge in mm year^{-1}. The precipitation and discharge information for the water balance approach were selected and used as explained below.

505

Ensemble satellite precipitation

The challenge posed by using satellite-based precipitation data in African catchments is that most, if not all, satellite precipitation products are geographically biased towards either underestimation or overestimation, despite some of them having good correlation with ground

510   observations (i.e., Macharia *et al.,* 2022; Asadullah *et al.*, 2008; Dinku *et al.,* 2007). The lack of adequate ground precipitation observations makes it difficult to validate, as well as correct, the product(s') biases with a good degree of certainty. There is not a single precipitation product that has been found to perform better than other precipitation products across African landscapes and southern Africa in particular (i.e., Macharia *et al.,* 2022). For the Luangwa Basin there is no

515   guarantee any of the precipitation products are spatially representative of a basin that is about 159,000 square kilometres with varying topographical attributes. For instance, compared to point-based field observations of precipitation at six weather stations in Zambia (three stations in the Luangwa Basin and the other three outside of the Luangwa Basin) no single satellite-based precipitation produc~~tion~~ showed consistency with either underestimating or overestimating

520   precipitation across all weather stations (see Table A1 in the supplementary data). Using an ensemble of precipitation products is said to reduce errors and therefore, recommended (i.e., Weerasinghe *et al.*, 2020; Asadullah *et al.*, 2008). When the annual mean of an ensemble of four satellite-based precipitation products was compared to annual means of field observations at different weather stations the margin of either underestimation or overestimation was reduced (See

525   Table A1 in supplementary data). To ~~this extent, for the general water balance,~~ this study used annual mean of four satellite precipitation products. The four precipitation products are the Climate Forecasting System Reanalysis (CFSR), Climate Hazards Group Infra-Red Precipitation with Station data (CHIRPS), ECMWF Reanalysis v5 (ERA5) and TerraClimate (see Table 1). These satellite precipitation products were selected purely based on availability and the fact that they are

530   spatially distributed and cover~~s~~ the entire Luangwa Basin (Table 1). Field observations of precipitation for GART Chisamba (data for the period 2020 – 2022) and Lusaka International Airport, Kabwe, Mwinilunga and Serenje weather stations for the years 2014 - 2016 were obtained from the Southern African Science Service Centre for Change and Adaptive Land Management (SASSCAL) weathernet (Last accessed: 20 January, 2023: http://www.sasscalweathernet.org).

535   The observations for Mpika for the year 2021 were obtained from the ZAMSECUR project dataset available at 4TU.ResearchData repository (https://doi.org/10.4121/19372352.v2) (Zimba *et al.,* 2022). Three weather stations, GART Chisamba, Lusaka International Airport and Mwinilunga, are outside of the Luangwa Basin and were used for comparison purposes only. However, GART and Lusaka International airport stations are very close to the Luangwa Basin. The other three

540   stations Kabwe, Serenje and Mpika are within the Luangwa Basin (see Table A1 in the supplementary data for location coordinates of the weather stations). However, the results of the comparison of satellite precipitation products with field observations were similar

(underestimation or overestimation) at all weather stations both in the Luangwa Basin and outside
the basin (See Table A1 in the supplementary data).

545

Estimating runoff data

Reliable monthly basin-scale field observations of runoff were only available for the period
1961 -1992 and not for the study period 2009 – 2020. Monthly modelled TerraClimate runoff data
(Abatzoglou *et al.,* 2018) was available for the period 1958 – 2020. Compared to field observations
550 TerraClimate runoff data was significantly higher during the peak rainfall period of January-
February. At annual scale TerraClimate overestimated runoff data but strongly correlated (r = 0.83)
with field observations (Fig. 4a).

555
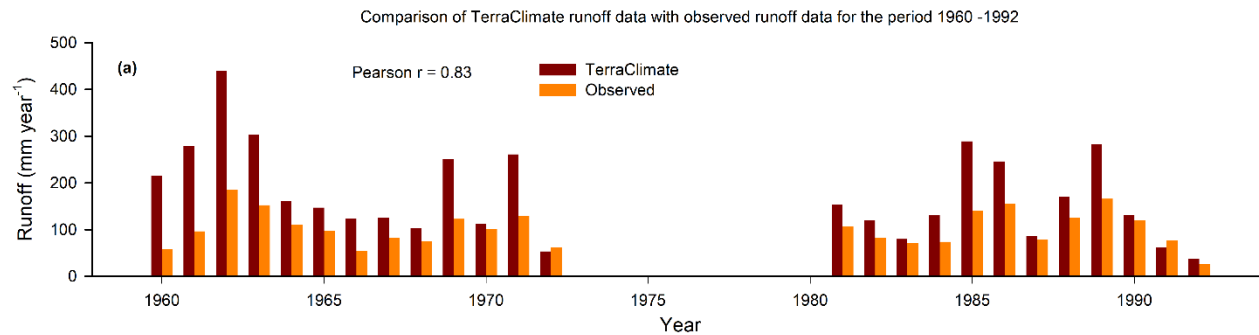
560
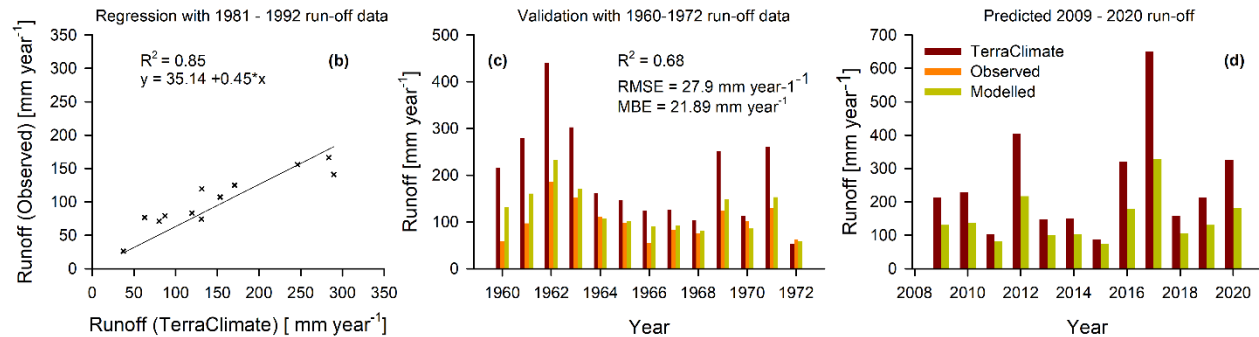
565

570

Figure 4: Procedure for extending near field observations runoff data for the period 2009-2020
using the TerraClimate runoff data as the predictor.

Based on the correlation of annual TerraClimate runoff data with field observations a linear
575 regression equation was formulated to help generate extended near field observations time series
for the period 2009-2020. TerraClimate runoff data was used as predictor variable. The
TerraClimate runoff data was used because of availability free of cost and with relatively fine
temporal and spatial resolution (monthly and 5 km respectively) (Table 1). Firstly, the field
observations runoff data and TerraClimate runoff data for the period 1960 - 1992 were split into
580 two segments, 1960 - 1972 and 1981 - 1992. The runoff data for the period 1981 -1992 was used
as training data to generate a linear equation with the TerraClimate runoff data as the predictor
variable (Fig. 4b). The generated linear equation was validated using the 1961-1972 TerraClimate
runoff data as a predictor variable (Fig. 4c). The predicted 1961-1972 runoff data with the
TerraClimate runoff data as a predictor variable was then compared to the field observations for
585 the same period (Fig. 4 c). The performance statistics of the equation showed $R^2 = 0.68$, RMSE =

27.90 mm year^{-1} and mean bias error (MBE) = 21.89 mm year^{-1} (Fig. 4 c). The validation results of the regression equation were deemed sufficient for this study. The linear regression equation was then used to generate near field observations runoff data for the period 2009 – 2020 with TerraClimate runoff data for the same period as the predictor variable (Fig. 4 d). Generally, both observed and extended (with TerraClimate data as predictor) annual runoff was, on average, 11 percent of annual satellite-based precipitation. The ~~near field observations~~ extend runoff data was then used in the water balance approach, as explained in Section 2.5, to estimate actual evaporation at basin level.

2.2.5 Statistical analyses

The coefficient of variation C_v (%) in Eq. (2) (Helsel *et al.*, 2020) was used to understand the extent to which the satellite-based evaporation estimates varied among each other in each phenophase. Furthermore, the analysis of variance (ANOVA) (Helsel *et al.*, 2020) and all pairwise multiple comparison procedures with the Tukey Test (Helsel *et al.*, 2020) were performed. The all pairwise comparison assisted in observing the satellite-based evaporation estimates that were significantly similar or different in magnitudes in each phenophase. The correlations (similarity in trends) among satellite-based evaporation estimates were assessed at monthly and annual scales using a non-parametric technique the Kendal correlation test (Helsel *et al.*, 2020). To establish the extent to which the satellite-based evaporation estimates underestimated or overestimated evaporation, relative to E_{wb}, the mean bias (Eq. 3) was used.

$$C_v = \frac{\bar{x}}{\bar{s}} * 100 \tag{2}$$

where $\bar{x}$ is the standard deviation and $\bar{s}$ is the mean of the observations. The higher the C_v value, the larger the standard deviation compared to the mean, which implies greater variation among the variables.

$$MBE = \frac{1}{n}\sum_{i=1}^{n}(E_{s_i} - E_{a_{(wb)}}{}_i) \tag{3}$$

where n = number of observations, $E_{a\,(wb)}$ = water balance-based actual evaporation time series and E_s is the satellite-based evaporation estimates time series. The smaller the mean bias value (positive or negative), the less the deviation of the predicted values from the observed values (Helsel *et al.*, 2020).

3 Results and discussion
3.1 Basin scale miombo woodland climate and phenological trend(s)

Figure 5 shows Luangwa Basin miombo woodland aggregated 2009-2020 MODIS NDVI and CFSR data climate conditions; net radiation (R_N), air temperature (T_a), relative humidity (RH), soil moisture (SM) and precipitation (P). The peak atmospheric and phenological variables values were observed in the early and mid-rainy seasons during the green-up and maturity/peak phenophases. The lowest values in atmospheric and phenological variables were observed in the cool dry season during the green-down and dormant phenophases. Net radiation, air temperature, relative humidity covaried (positively or negatively) with the NDVI (proxy for canopy phenology) depending on the phenophase (Fig. 5 and Fig. A2 in the supplementary data).
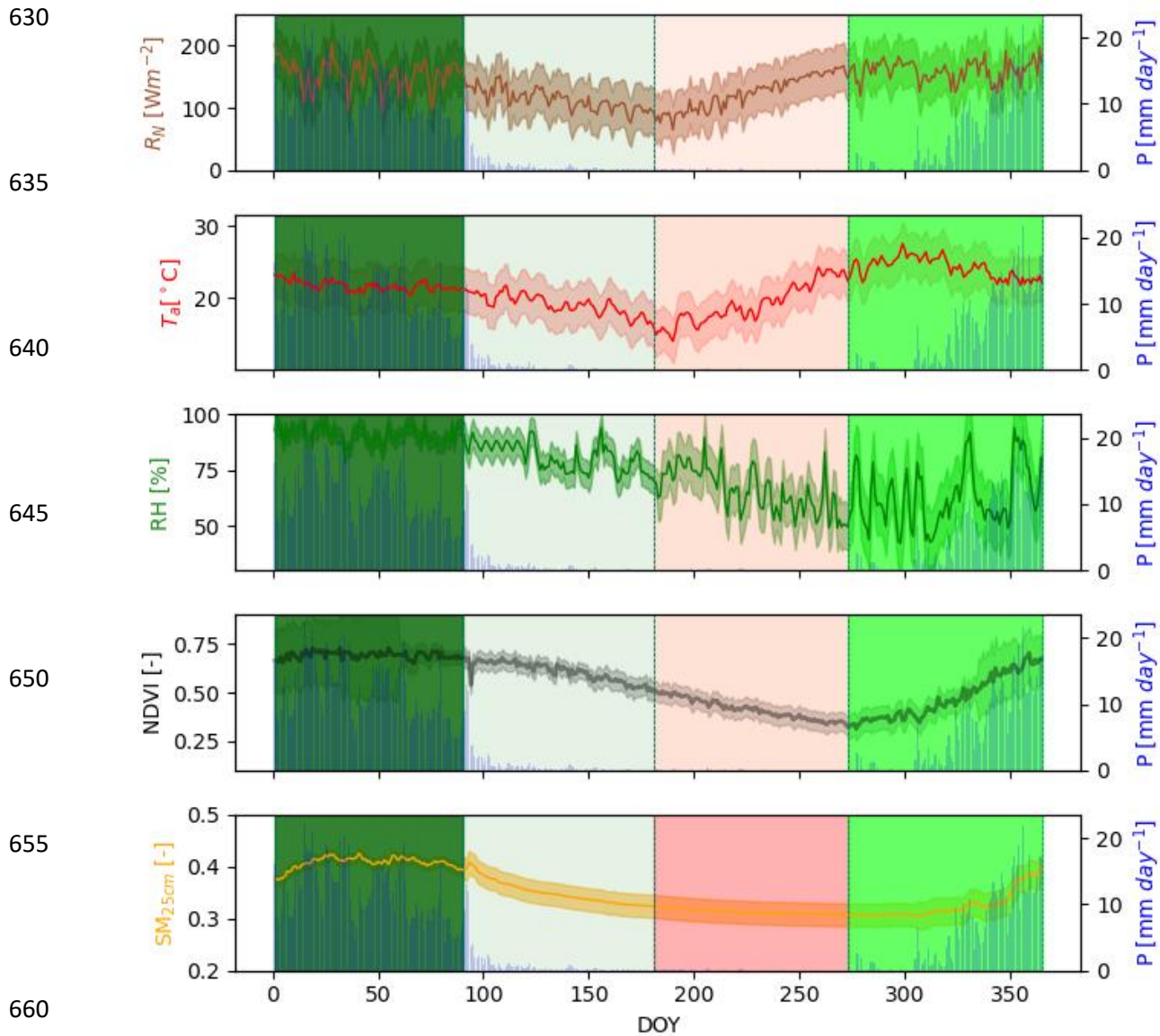
Figure 5: Luangwa Basin miombo woodland spatially and temporally aggregated 2009-2020 daily atmospheric conditions net radiation (R_N), precipitation (P), relative humidity (RH) and air temperature (T_a); phenological conditions proxied by the NDVI; and soil moisture (SM). The shaded areas represent the phenophases as used in this study: January – March is the peak/maturity, April – June is the senescence/green-down, July – September is the dormant and October – December is the green-up/mid-green-up phenophase. Shaded area for variables is the standard deviation. DOY is the day of the year.

The strong correlation between climate and phenology (i.e., NDVI and air temperature/soil moisture) in the miombo woodland (Fig. A2 in the supplementary data) agreed with observations made by Chidumayo (2001) and in other ecosystems (Pereira *et al.*, 2022; Niu *et al.*, 2013; Cleland *et al.*, 2007).

3.2 Observed phenological conditions in the miombo woodland

It was observed that the canopy closure is varied, ranging between 2 percent to about 70 percent in the shrub, dry miombo woodland and wet miombo woodland (Fuller, 1999). Therefore, depending on location and dominant species exposure of the understory, field and ground layers to incident solar radiation, through the canopy is substantial (Fig. 6, Chidumayo, 2001; Fuller, 1999).

Figure 6: Dry season (a) and rainy season (b) tree layer, understory and field layer conditions at the wet miombo woodland site in Mpika, Zambia. Images taken on 29th September and 23rd December, 2021.

The field layer during the rainy season mainly comprises green grass (Fig. 6b and Chidumayo, 2001). Therefore, total LAI and NDVI in phenophases in the rainy season can be largely attributed to both the field layer i.e., grass, understory and the tree layer i.e., shrubs and tree canopy (i.e., Fig. 6b and Chidumayo, 2001). In the dry season the grass in the field layer and some understory non-deep rooting shrubs dry out (Fig. 6a and Chidumayo, 2001, Fuller, 1999). Therefore, the changes in total LAI and NDVI in the phenophases in the dry season can largely be attributed to the changes in the tree layer of the miombo species (i.e., Fig. 6a, Fig. 7 and Chidumayo, 2001).

The LAI and NDVI were used as proxies to observe the changes in the canopy cover across different phenophases of the miombo woodland. At pixel scale the spatial distribution and mean values of the LAI and NDVI for the wet miombo woodland differed with that for the dry miombo woodland (Fig. 8a). This is due to the differences in the miombo species composition and distribution at each site. Furthermore, there are differences in soil type, soil moisture, temperature, nutrients, rainfall and canopy closure at the two sites (i.e., Chidumayo, 2001; Fuller, 1999). However, trends in the NDVI and LAI across different phenophases of the miombo woodland at the two sites were significantly similar (Pearson r = 0.73 for LAI and NDVI respectively) (Fig. 8b). Highest LAI and NDVI, both in the dry miombo woodland and wet miombo woodland, were observed in the maturity/peak phenophases during the mid-rainy season (January – March) (Figs. 5, 7 & 8b). This period for peak LAI and NDVI (Figs. 7 & 8) agrees with Chidumayo (2001) who observed that peak green biomass in the miombo woodland occur anytime between January and May. The lowest LAI and NDVI were observed in the dormant phenophase in August/September during the warm pre-rainy season (Figs. 5, 7 & 8).
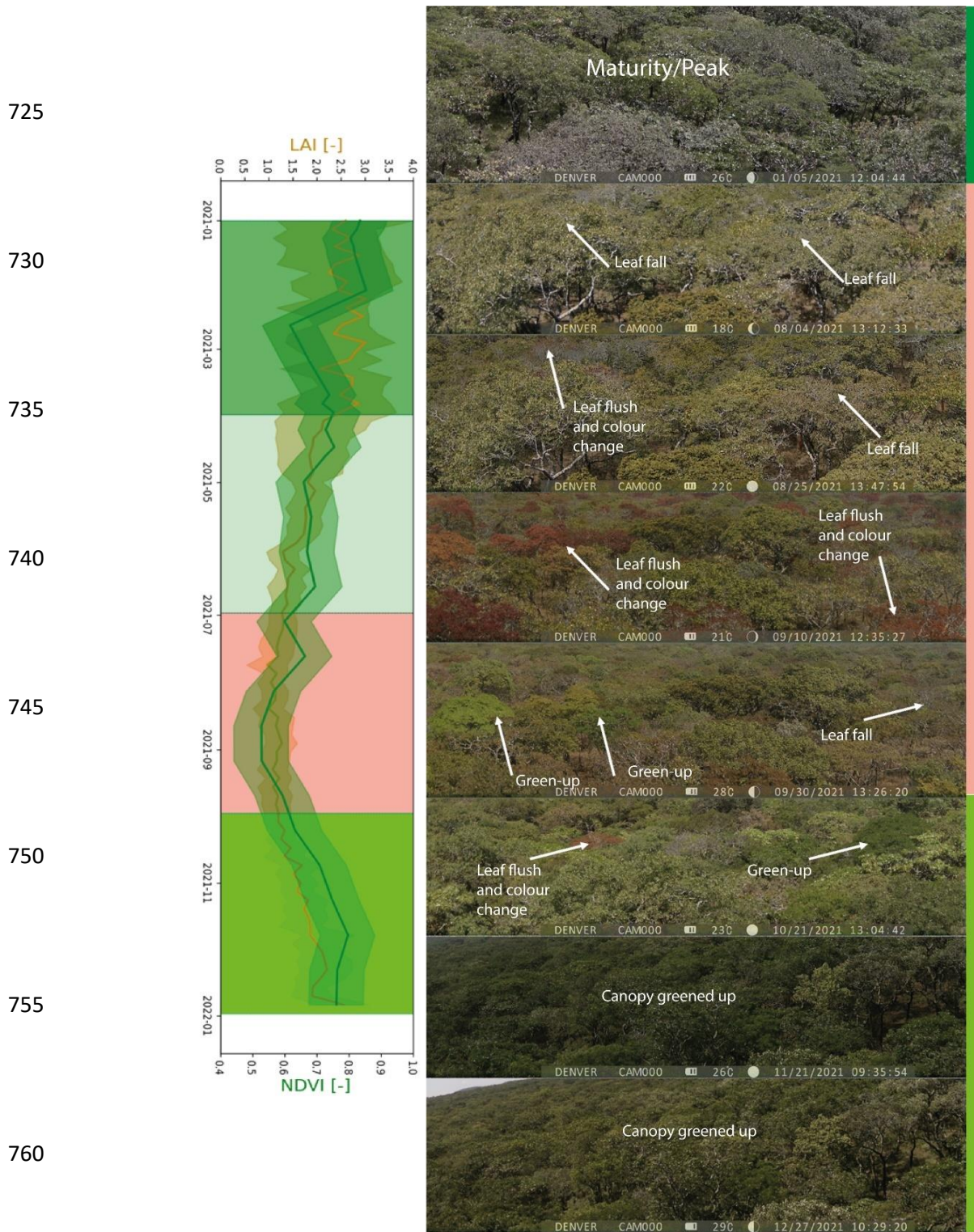
Figure 7: Temporal trend of MODIS *LAI*, *NDVI*, and the wet miombo woodland canopy display trend for the year 2021 at Mpika study site. Shaded area are phenophases: January – March is the Maturity/Peak; April-June is the Senescence/Green-down; July-September is the Dormant while October – December is the green-up. Shaded area for variables is the minimum and maximum.
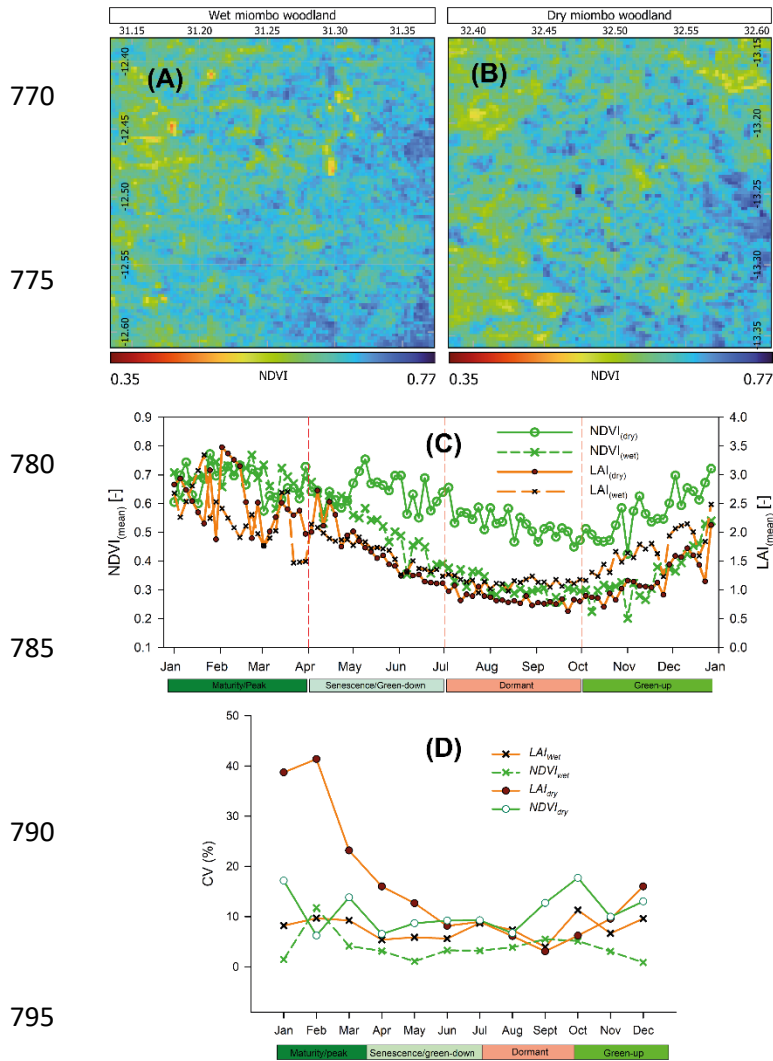
Table 2. Dormant phenophase CV correlation

Variables	LAI (wet)	NDVI (wet)	LAI (dry)	NDVI (dry)
LAI (wet)	**1**			
NDVI (wet)	**-1.00**	**1**		
LAI (dry)	0.98	-0.98	**1**	
NDVI (dry)	-0.75	0.75	-0.59	**1**

Figure 8: Spatial distribution of NDVI at the (A) wet miombo woodland and (B) dry miombo woodland site for the period January-December, 2021. (C) Temporal distribution of the LAI and NDVI for the wet miombo woodland and dry miombo woodland. (D) Coefficients of variation in the LAI and NDVI values at the wet miombo woodland and dry miombo woodland in the Luangwa Basin in Zambia for the year 2021.

The leaf fall, leaf flush and changes in colour of the leaves intensifies in the August-September period (Fig. 7, Chidumayo, 2001; Chidumayo and Frost, 1996; Fuller, 1999). The intensified leaf fall, leaf flush and leaf colour changes may also explain the increased variations in the NDVI values in August-September (Fig. 8d). Table 2 shows the correlation coefficients of the coefficients of variations in NDVI and LAI values for the dry miombo woodland and wet miombo woodland.
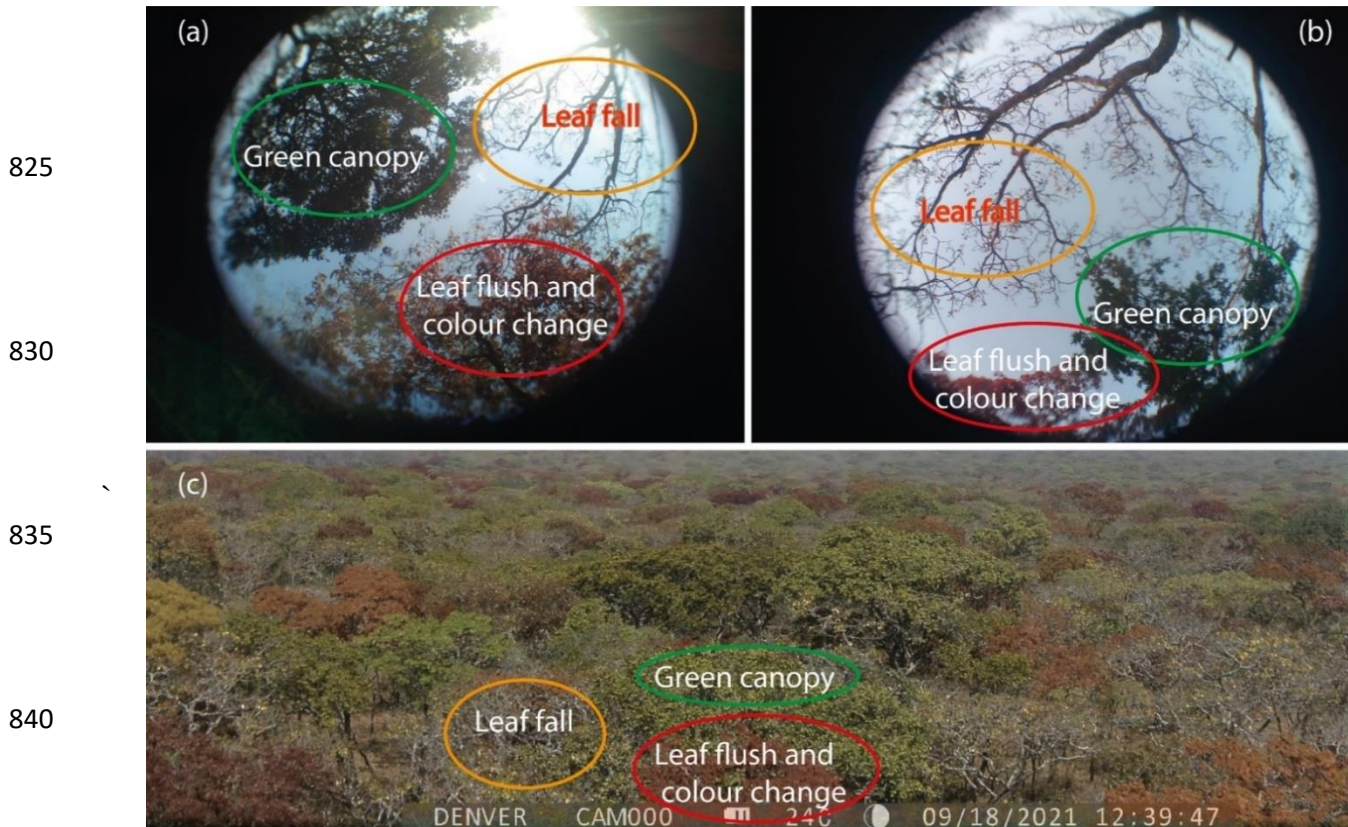
Figure 9: Heterogeneity in leaf fall and leaf flush activities among miombo woodland species: observed from under the canopy (a, b) and as observed above the canopy (c). Images taken at the wet miombo woodland site in Mpika, Zambia. Images taken on 18 September, 2021.

The coefficients of variation in LAI and NDVI values for the dry miombo woodland and wet miombo woodland were only similar for the dormant phenophase (Pearson r = 0.98 and 0.75 for the LAI and NDVI respectively (Fig. 8 and Table 2). The similarity in the coefficients of variations of estimates for the dry miombo woodland and wet miombo woodland LAI and NDVI values in the dormant phenophases may be due to the miombo plants at the two sites undergoing similar phenological processes; leaf fall and leaf flush. In the dormant phenophase the grass component would have dried out leaving largely the tree component (i.e., miombo plants canopy) (Chidumayo, 2001).

The coefficients of variation in LAI values in July and August in wet miombo woodland can be attributed to increased leaf fall activity (Fig. 8). Fuller (1999) observed that in the wet miombo woodland the simultaneous occurrence of the leaf fall and leaf flush, in August and September, among miombo species resulted in net zero change in the canopy closure. The net zero

860 change increase in canopy closure may explain the observed low coefficient of variation in the LAI values in September (Fig. 8). The substantially high coefficient of variations in LAI and NDVI values, for both dry miombo woodland and wet miombo woodland, during the mid-rainy season in the maturity/peak phenophases mainly can be attributed to two factors. Firstly, the increase in the growth of the green biomass of the woodland which occur anytime between January and May

865 (Chidumayo, 2001, Fuller, 1999) and the effect of cloud cover on the quality of the satellite-based LAI and NDVI products (Vermote and Wolfe, 2015; Zang *et al.,* 2003). Furthermore, the differences in the canopy closure between the dry miombo woodland and wet miombo woodland (Fuller, 1999) may be the reason for differences between the coefficients of variations in LAI and NDVI values in the maturity/peak and senescence\green phenophases. For instance, the dry

870 miombo woodland which has a lower canopy closure compared to the wet miombo (Fuller, 1999) is likely to have a higher grass component. Additionally, the differences in miombo species composition, distribution of rainfall, soil type and soil moisture, among other variables, may result in varied phenological differences between the dry miombo woodland and wet miombo woodland (Chidumayo, 2001; Fuller, 1999). However, unlike in the other phenophases, there appeared strong

875 correlations (Table 2) in the variations in LAI and NDVI values in the dry miombo woodland and wet miombo woodland in the dormant phenophase. The simultaneous occurrence of leaf fall and leaf flush (i.e., Fig. 9) is one of the phenological attributes that distinguishes the miombo woodland from other woodlands (Fuller, 1999; White, 1983). The leaf fall and leaf flush in the dry season (Figs. 7 & 9) occur many weeks and even months before the start of the rains. The growth of the

880 new leaves in the dry season is sustained by both access to deep soil moisture, including ground water, and the adapted plant water storage mechanisms (i.e., Tian *et al.,* 2018; Vinya *et al.,* 2018; Fuller, 1999; Savory, 1963). The leaf fall and leaf flush occur simultaneously (i.e., Fig. 9) and results in net zero change increase in canopy closure in the dry season in wet miombo woodland (i.e., ~~miombo woodland site in~~ Mpika) (Fig. 9 and Fuller, 1999). The balance in the leaf fall and

885 leaf flush may explain the lower coefficient of variation in LAI values in September in both dry miombo woodland and wet miombo woodland. Therefore, in the dormant phenophase and the early green up in October, when the total LAI and NDVI can largely be attributed to the miombo woodland plants, the variations in the trend in the changes in phenology appear to be similar in both dry miombo woodland and wet miombo woodland, though at different rates (Fig. 8).

890

3.3 Phenophase-based difference in satellite-based evaporation estimates

The correlation coefficients revealed that trends in satellite-based evaporation estimates at pixel scale (dry miombo woodland and wet miombo woodland) and the Luangwa Basin scale were similar (Fig. 10). The results of the ANOVA showed no statistically significant (p-values > 0.05)

895 differences in the magnitudes of each satellite-based evaporation estimate between the dry miombo woodland and wet miombo woodland (Fig. A4 and Table A2 in the supplementary data).

Overall, for the hydrological year (September – August, as shown in Fig. 10) all satellite-based evaporation estimates showed positive correlation (i.e., similar trend) with the NDVI (proxy for changes in the phenology) (Fig. 10 d); though in the dormant and maturity/peak phenophases

900 some satellite-based evaporation estimates showed negative correlation with the NDVI (Fig. A3 in the supplementary data).

Among satellite-based evaporation estimates significant differences (r <0.5, *p-value <* 0.05) in trends were observed more in the dormant phenophase in the dry season and partly in the maturity phenophase in the rainy season.

905
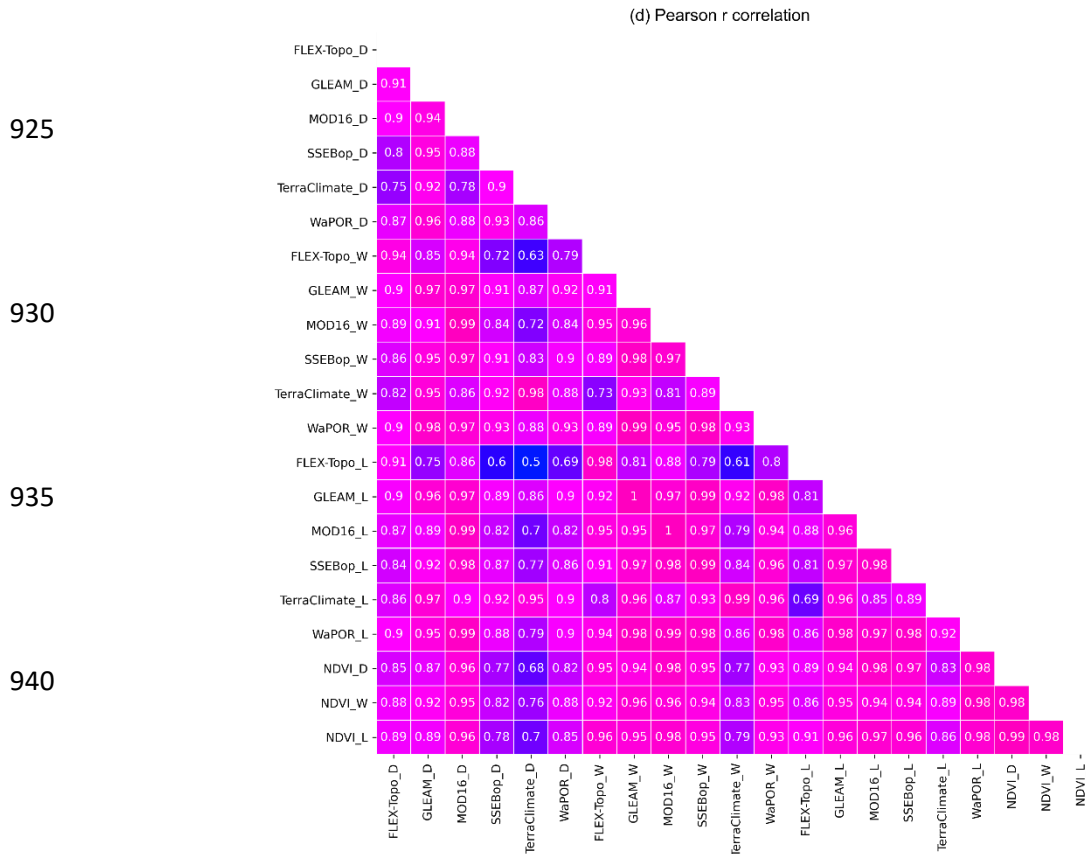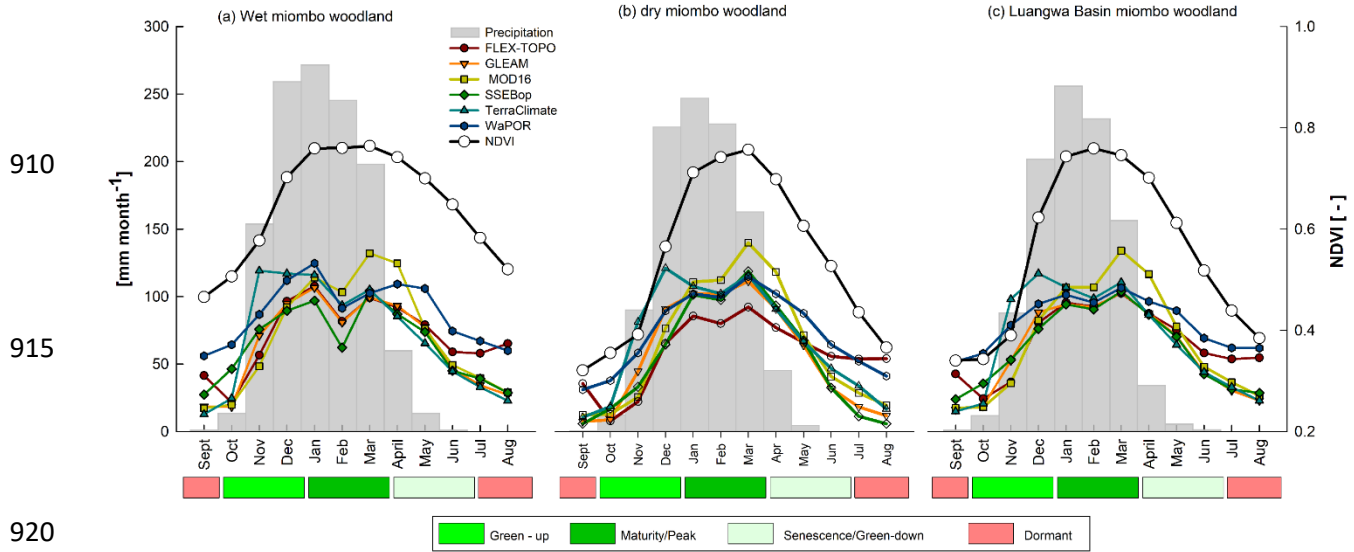
Figure 10: Comparison of aggregated 2009-2020 satellite-based evaporation estimates in relation to the NDVI (a) at wet miombo woodland, (b) dry miombo woodland, (c) delineated Luangwa Basin miombo woodland across hydrological year (September – August) in the Luangwa Basin and (d) Correlation of aggregated monthly satellite-based evaporation estimates and NDVI at pixel level (D = dry miombo woodland pixel, W = wet miombo woodland pixel) and Luangwa Basin scale (L = Luangwa Basin miombo woodland).
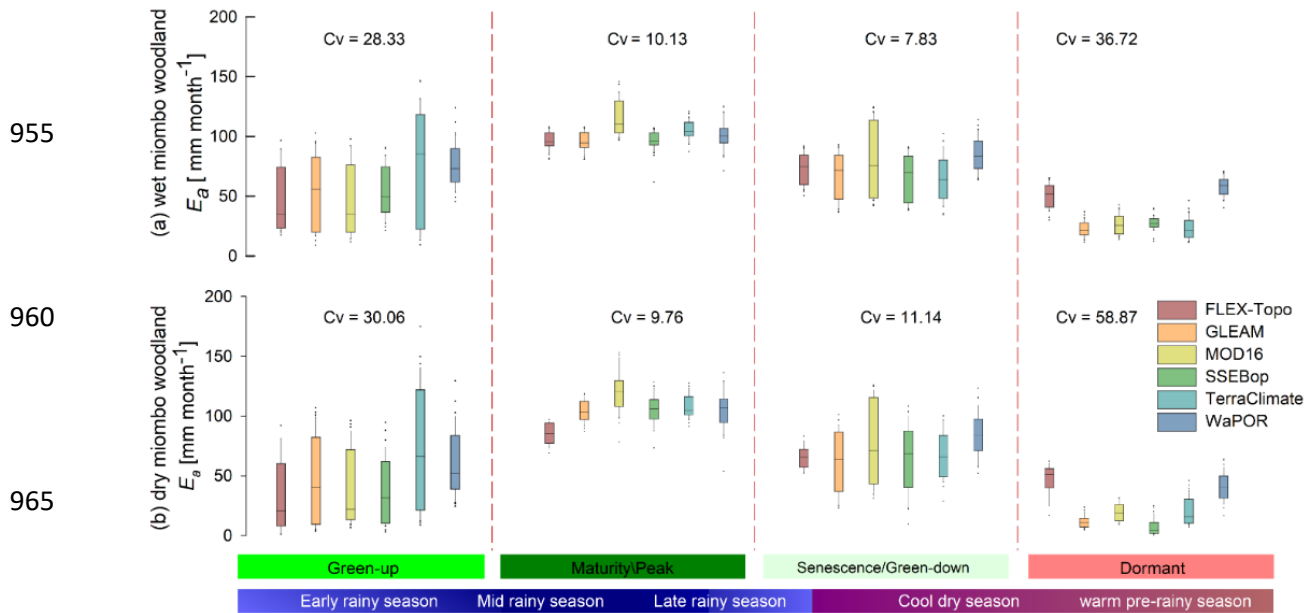
Figure 11: Comparison of satellite-based evaporation estimates across phenophases based on hydrological year (a) in wet miombo woodland and (b) in dry miombo woodland. Most variations in actual evaporation estimates among the satellite-based evaporation estimates were observed in the dormant and green up phenophases.

In the dormant phenophase, FLEX-Topo and WaPOR had, generally, lower correlations with the rest of the satellite-based evaporation estimates (Fig. A3 in the supplementary data). In the maturity/peak phenophase in the rainy season MOD16 and SSEBop showed most lower correlations with other satellite-based evaporation estimates. The green-up phenophase and senescence/green-down phenophase showed higher correlation coefficients ($r > 0.6$) among all satellite-based evaporation estimates (Fig. A3 in the supplementary data).

Substantial differences in the means of satellite-based evaporation estimates, at both pixel level in the dry wet miombo woodland, wet miombo woodland and at the Luangwa Basin miombo woodland scale, were observed during the green-up (C_V = 28.23; 30.06; 22.63 percent, respectively) and dormant phenophase (C_V =36.72; 58.87; 39.98 percent, respectively) (Figs. 10, 11 & Table A3 in the supplementary data). For the green-up phenophase the meaning of the coefficients of correlation and coefficients of variations in evaporation estimates is that while the trends among the satellite-based evaporation estimates are significantly similar the amounts are significantly different. In contrast, for the maturity/peak phenophase the trends among some satellite-based evaporation estimates are not similar (Fig. A3 in the supplementary data) but the magnitudes are similar (Fig. 11). For the senescence/green-down phenophase both the trends and magnitudes of satellite-based evaporation estimates are significantly similar. The results for the senescence appear to agree with the findings by Zimba *et al.* (2023) in which they showed, at point scale, that the trends and magnitudes of satellite-based evaporation estimates were similar to each other and also to the field observations of actual evaporation of the wet miombo woodland.

For the dormant phenophase most of the trends and magnitudes of satellite-based evaporation estimates were significantly different. In the dormant phenophase in the dry season the FLEX-Topo and WaPOR showed higher estimates of evaporation compared to other satellite-based evaporation estimates (Fig. 11 a, b). Zimba *et al.* (2023) showed, at point scale in the wet

miombo woodland, that satellite-based evaporation estimates underestimated actual evaporation in the dry season. They also showed that while the NDVI was generally in a downward trajectory from May to September, the observed actual evaporation had a rising trajectory which was in tandem with the rising air temperature and net radiation. Compared to other satellite-based estimates the WaPOR followed the same trend as the field observations of actual evaporation of the wet miombo woodland in the dry season (Zimba *et al.,* 2023). In this study FLEX-Topo and WaPOR showed negative correlation with the NDVI in the dormant phenophase in the dry season (Fig. A3 in the supplementary data). Therefore, with reference to findings by Zimba *et al.* (2023) and Figs. 11 & A3 in the supplementary data, the FLEX-Topo and WaPOR appear to have the correct trend of actual evaporation of the miombo woodland in the dormant phenophase in the dry season.

The green-up phenophase is at the commencement of the rain season with high canopy cover (i.e., mean NDVI between 0.5 and 0.7) and highest net radiation (i.e., 150 Wm^{-2}) (Figs. 5 & 10). The dormant phenophase is during the driest part of the year with the lowest moisture in the topsoil, least woodland canopy cover (i.e., NDVI ≈ 0.5) but, compared to the senescence/green-down phenophase, with increasing net radiation and air temperature (Fig. 5). What is important to note is that, unlike during the maturity/peak and senescence/green down phenophases, the total LAI and total NDVI during the dormant and green-up phenophases can largely be attributed to the tree layer (i.e., miombo woodland canopy) (Chidumayo, 2001; Chidumayo and Frost, 1996). The implication is that the dormant and green-up phenophases are likely to be more representative of the evaporation of the miombo species than the other phenophases in the rainy season when the grass component substantially increases. Compared to the maturity/peak and the senescence/green-down phenophases, the dormant and green-up phenophases showed higher coefficients of variations in evaporation estimates among satellite-based evaporation estimates (Fig. 11 and Fig. A4 in the supplementary data). The substantial differences (i.e., coefficients of variations in estimates) in satellite-based evaporation estimates during the dormant and green-up phenophases suggests that there are aspects of the evaporative processes (i.e., phenology-water interactions) of the miombo species that are possibly not substantially taken into account in satellite-based evaporation estimates. The possible explanations for the observed trends (correlations) and coefficients of variations in satellite-based evaporation estimates are given in section 3.8.

3.4 All pairwise multiple comparison of satellite-based evaporation estimates at Luangwa Basin miombo woodland scale

Tables A4 in the supplementary data shows a summary of results of the ANOVA and all pairwise multiple comparison of satellite-based evaporation estimates. The six satellite-based evaporation estimates are compared with each other in each phenophase. The number of times each satellite-based evaporations estimate is different from the other five satellite-based evaporation estimates was observed as shown in Fig. 12.

In the dormant phenophase the magnitudes of FLEX-Topo and WaPOR were significantly (p-value > 0.05) similar to each other but significantly (p-value < 0.05) different from the other satellite-based estimates. In the same phenophase GLEAM and MOD16 showed similar trends and magnitudes. SSEBop estimates were significantly different from MOD16 and TerraClimate estimates. The rest of the comparisons did not show significant differences in magnitudes of satellite-based evaporation estimates (Table A4 in the supplementary data). During the green-up phenophase there were no significant (p-value > 0.05) differences between GLEAM estimates and

FLEX-Topo estimates. SSEBop estimates were significantly (p-value < 0.05) different from FLEX-Topo and MOD16 estimates. The TerraClimate and WaPOR estimates were significantly different (p-value < 0.05) from other estimates (Table A4 in the supplementary data). In the maturity/peak phenophase MOD16 was significantly (p-value < 0.05) from the other satellite-based evaporation estimates. During the same period GLEAM, SSEBop and WaPOR were significantly different from at least one other satellite-based estimate (Table A4 in the supplementary data).

No. of times each SEE differ significantly with other SEE

Figure 12: Number of times each satellite-based evaporation estimate (SEE) was significantly different to one or more other SSE in each phenophase at Luangwa Basin miombo woodland scale.

During the senescence/green-down phenophase the WaPOR significantly differed with FLEX-Topo, GLEAM, SSEBop and TerraClimate while the rest of the comparison showed similarity in magnitudes among satellite-based evaporation estimates. Across phenophases WaPOR showed the highest frequency of being significantly different from other satellite-based evaporation estimate followed by FLEX-Topo, MOD16 and TerraClimate (Fig. 12 and Table A4 in the supplementary data).

3.5   Variations within each climate, LAI, NDVI and satellite-based evaporation estimate

With an exception of WaPOR, variations in within satellite-based evaporation estimates were highest in the green-up phenophase followed by the dormant and senescence/green-down phenophases (Fig. 13a). The maturity/Peak showed the least coefficients of variations in within satellite-based evaporation estimates (Fig. 13a and Table A3 in the supplementary data). The green-up and senescence/green-down phenophases are at the boundaries of the dry season into the mid-rainy season (in case of green-up phenophase) and the rainy season into the dry season (in the case of the senescence/green-down phenophase). The coefficients of variations in the NDVI (i.e.,

canopy cover), rainfall (i.e., water availability) and temperature (i.e., energy availability) values in the green-up and senescence/green-down phenophases (Fig. 13b) likely explains the variations within each satellite-based evaporation estimates (Table A3 in the supplementary data). The variations in within satellite-based evaporation estimates in the dormant phenophase could be due to the changes in the canopy cover (i.e., NDVI as shown in Fig. 13b) due to the leaf fall, leaf flush and leaf colour changes.
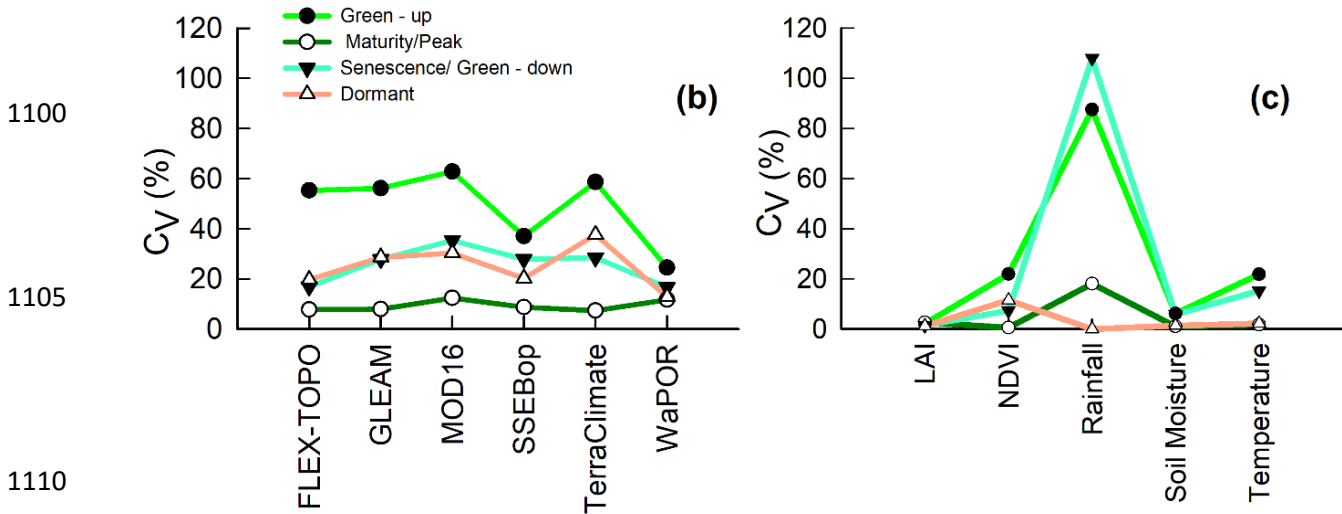
Figure 13: Coefficients of variations (a) showing within satellite-based evaporation estimate variations across phenophases and (b) within variations in estimates for atmospheric and phenological variables across phenophases at Luangwa Basin miombo woodland scale.

In the dormant phenophase in the dry season FLEX-Topo, SSEBop and WaPOR showed lower within estimates coefficients of variations compared to GLEAM, MOD16 and TerraClimate (Fig. 13a). The maturity/peak phenophase showed the lowest within estimates coefficients of variation in satellite-based evaporation estimates, LAI, NDVI, rainfall, soil moisture and temperature (Fig. 13). Figure 13 generally shows that, among many other influencing factors, the variations in trends and magnitudes of LAI, NDVI, rainfall, soil moisture and air temperature are mirrored in the variations in the satellite-based evaporation estimates.

3.6 Differences in spatial distribution of satellite-based evaporation estimates

Figure 14 shows spatial-temporal distribution of satellite-based evaporation estimates across different phenophases for the hydrological year 2019/2020. The comparison was based on the entire Luangwa Basin, including non-miombo woodland regions. Generally, the spatial distribution of evaporation in all satellite-based evaporation estimates was different (Fig. 14). However, substantial differences in the spatial distribution of actual evaporation among the satellite-based evaporation estimates were more visible in the dormant and green-up phenophases (Fig. 14). During the dormant phenophase, all six satellite-based evaporation estimates appeared to show higher actual evaporation in miombo woodland areas than in other land cover types (Fig. 14) (refer to Fig. 1 b, c for distribution and extent of the cover of the miombo woodland in the Luangwa Basin). Potential contributing factors to the observed differences in spatial-temporal distribution of satellite-based evaporation estimates are highlighted in section 3.8.
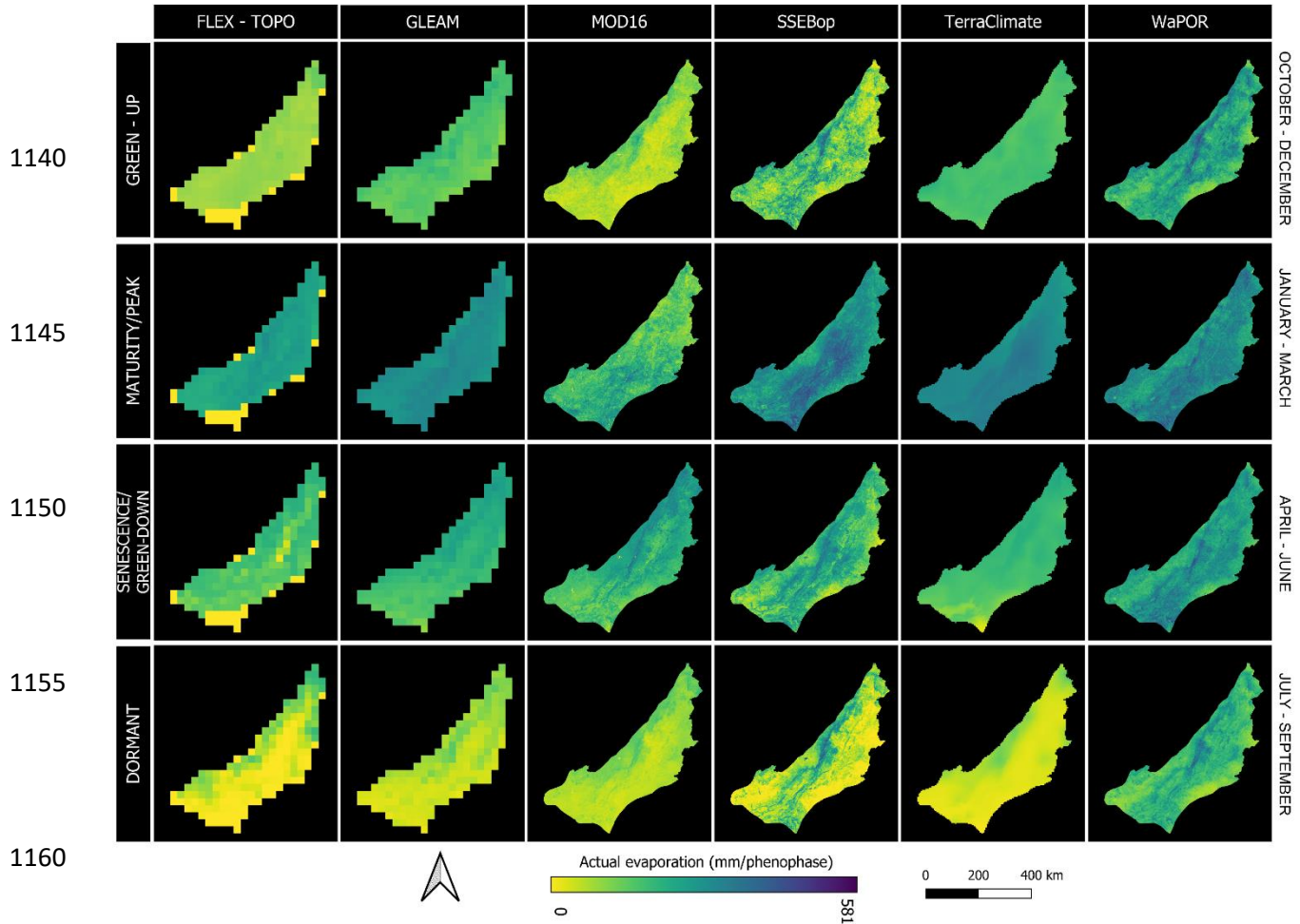
Figure 14: Spatial-temporal distribution of satellite-based evaporation estimates across different vegetation phenophases of the Luangwa Basin for the hydrological year September 2019- August 2020.

3.7 Comparison of satellite-based evaporation estimates to the water balance-based actual evaporation estimates

Figure 15 shows the results of the temporal comparison of satellite-based evaporation estimates with the water balance-based evaporation estimates at Luangwa Basin scale for hydrological years for the period September 2009 to August 2020. This comparison included non-miombo woodland areas. All satellite-based evaporation estimates showed insignificant correlation (*p-value* > 0.05) with the water balance-based actual evaporation (E_{wb}) (Fig. A5 in the supplementary data). The poor correlation could be due to the uncertainties in the precipitation and runoff data used in the study. It could also be that the satellite-based evaporation simply differs to actual Luangwa Basin actual evaporation each year. Compared to the E_{wb} estimates, all six satellite-based evaporation estimates underestimated actual evaporation (Fig. 15). Potential reasons for the underestimation include the quality of the precipitation product(s) used in this study. It is possible that despite the approach to minimise the margin of error by the use of the mean of four satellite-based precipitation products the precipitation was overestimated resulting in overestimating the actual evaporation with the water balance equation.
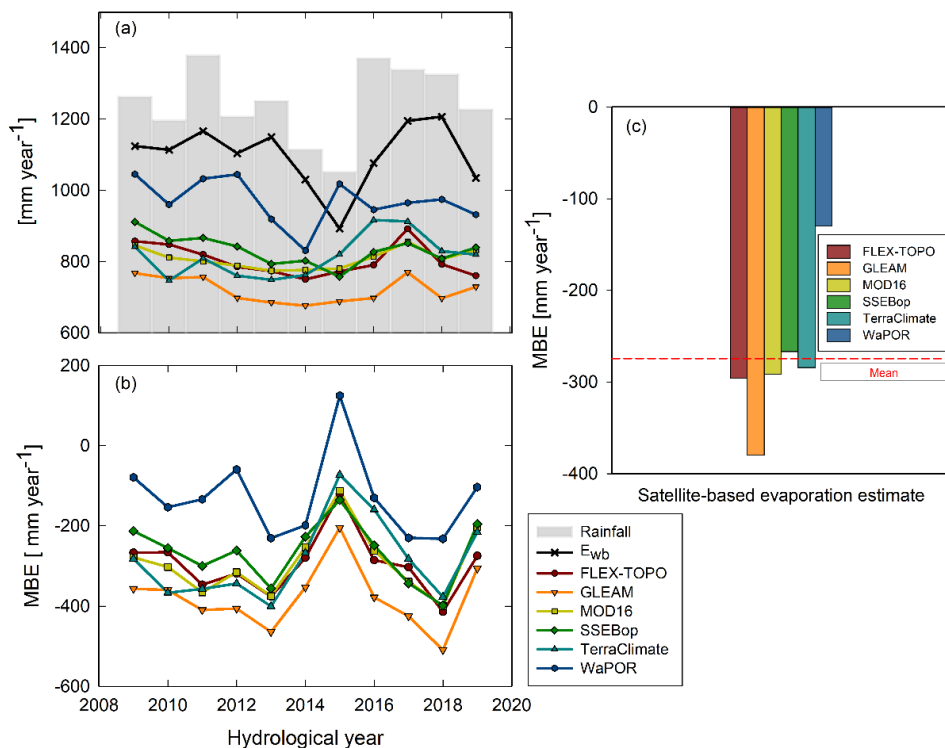
Figure 15: (a) Comparison of satellite-based evaporation estimates to the water balance-based estimates of actual evaporation for the Luangwa Basin, and (b) comparison of the MBE of satellite-based evaporation estimates and (c) comparison of the average MBE of individual satellite-based evaporation estimates to the average MBE of all six satellite-based evaporation estimates.
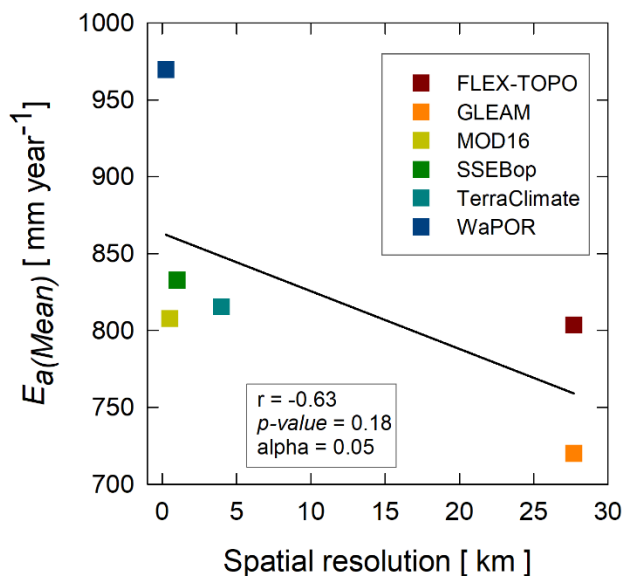
Figure 16: Basin scale correlation of actual evaporation estimates with spatial resolution of satellite-based evaporation estimates.

To the contrary the extended runoff time series with TerraClimate could have been overestimated resulting in underestimating the water balance-based actual evaporation at basin scale. The assumption of overestimation of the extended runoff data is based on the validation results of the linear equation used to extend the runoff time series, which showed RMSE = 27 mm year^{-1} and MBE = 21 mm year^{-1}. In any given year, WaPOR appeared to have the least underestimation with an average MBE of 120 mm year^{-1}, while GLEAM had the largest underestimation with an average MBE of 370 mm year^{-1}. Only SSEBop and WaPOR showed average MBE values below the average of all six satellite-based evaporation estimates (in dotted red line) (Fig. 15 c). At basin scale, it appeared there was no statistically significant correlation (r = -0.63; *p-value* =0.18; alpha = 0.05) between spatial resolution of satellite-based evaporation estimates and evaporation estimates of each product (Fig. 16). For instance, TerraClimate, with a coarser spatial resolution, compared to finer spatial resolution products MOD16 and SSEBop, showed similar bias estimates. The MOD16 had a higher spatial resolution than SSEBop, but underestimated more. The FLEX-Topo had a coarser spatial resolution than MOD16 and SSEBop but exhibited higher estimates in the dormant phenophases (July-September) (Figs. 10 and 11). The lack of a clear significant relationship, between spatial resolution and actual evaporation estimates (Fig. 16), may imply that other factors such as the heterogeneity in the land cover (i.e., miombo woodland, mopane woodland, cropland, settlements etc), differences in model structure, processes and model inputs, as highlighted in Zimba *et al.* (2023) and section 3.8 in this study, may be the largest contributing factors of the observed differences in the actual evaporation estimates at basin scale. However, unlike the observations for the wet miombo woodland by Zimba *et al.* (2023) the underestimation of actual evaporation at basin scale by satellite-based evaporation estimates cannot be entirely attributed to the inaccuracies in the simulation of evaporation of the miombo woodland. The evaporation of other vegetation types, i.e., mopane woodland, that are also found in the Luangwa Basin have not been investigated. What the basin scale water balance-based comparison suggests is that the satellite-based evaporation estimates possibly underestimate actual evaporation even in other non-miombo woodland landscapes. However, this suggestion needs to be investigated because it's possible the satellite-based evaporation estimates would perform differently in each landscape or land surface such as grassland, shrubland, wetland and mopane woodland. Therefore, the extent to which each land surface i.e., miombo and mopane woodlands, contribute to the actual evaporation of the Luangwa Basin need to be investigated. For a more comprehensive understanding of the evaporation of the Luangwa Basin there is need for the assessment of the phenology-water interactions of each vegetation type and the accompanying potential influence on the evaporation dynamics of the basin. Nevertheless, the results of this study agreed with Weerasinghe *et al.* (2020) who showed that most satellite-based evaporation estimates generally underestimated evaporation across African basins (i.e., Zambezi Basin) though SSEBop and WaPOR showed mixed behaviour of both underestimating and overestimating. In this study, in comparison to other satellite-based evaporation estimates, SSEBop and WaPOR appeared to have lower underestimations. The lower underestimation by SSEBop and WaPOR agreed with the point scale field observations for the wet miombo woodland (Zimba *et al.*, 2023) and suggests the two estimates could be close to field actual evaporation of the miombo woodland and the Luangwa Basin.

3.8 Potential contributing factors to the observed differences/similarities in trends, magnitudes and spatial distribution of satellite-based evaporation estimates

The most differences in trends and magnitudes of satellite-based evaporation estimates of the miombo woodland have been observed in the dormant phenophase in the dry season (Figs. 10, 11 & A3 in the supplementary data). Evaporation of the miombo woodland in the dormant phenophase in the dry season is through transpiration (i.e., Tian *et al.,* 2018). The dominant phenological characteristics of the miombo species in the dry season are the simultaneous leaf fall, leaf flush and greening up before commencement of seasonal rainfall (Fig. 7; Chidumayo and Frost, 1996; Frost, 1996). The transpiration of the miombo woodland is influenced by the above highlighted phenological and physiological characteristics as studies have shown (i.e., Marchesini *et al.,* 2015; Snyder and Spano, 2013). For instance, for the miombo woodland, Tian *et al.* (2018) showed that the terrestrial groundwater storage anomaly (TWS) continued to decrease throughout the dry season, and was indicative that miombo trees used deep ground water during the period. The suggestion that miombo trees access ground water is supported by Savory (1963) who showed that miombo species are deep rooting beyond 5 m with capacity to access ground water. It appears that satellite-based evaporation estimates from models whose structure, processes and inputs take into account the highlighted phenology-water interactions in the dry season and early rainy season, especially the access to deep soil moisture, are likely to have the accurate trends and magnitudes of evaporation of the miombo woodland.

3.81 Use of proxies for soil moisture in evaporation simulation

Some studies have shown that direct integration of soil moisture rather than the use of proxies improves the accuracy of actual evaporation estimates (Brust *et al.,* 2021; Novick *et al.,* 2016). The challenge with the use of the proxies for soil moisture, for example, in surface energy balance models is that these are unable to fully account for changes in other factors that may influence sensible heat fluxes (Gokmen *et al.,* 2012). To improve on the accuracy of estimation of water and energy fluxes in regions with recurrent plant water stress, i.e., miombo woodland, Gokmen *et al.* (2012) suggested that the soil moisture be integrated in the surface energy balance models. For instance, for MOD16 the use of the relative humidity and vapour pressure difference as proxies for soil moisture maybe a source of uncertainty in estimating transpiration (Novick *et al.,* 2016). Direct integration of soil moisture into the MOD16 algorithm appeared to improve the accuracy of actual evaporation estimates (Brust et *al.,* 2021). The energy balance-based SSEBop does not explicitly consider soil moisture dependency and assumes that the variations in satellite-based land surface temperature and vegetation indices such as the NDVI accounts for the soil moisture (Senay *et al.,* 2013). TerraClimate uses the plant-extractable water capacity of soil for soil moisture input. However, the challenge ~~with the plant-extractable water capacity of soil~~ is in selecting the rooting depth. GLEAM only takes into account 2.5m of the sub-surface moisture linked to observed precipitation. However, transpiration in the FLEX-Topo and WaPOR (ETLook model) is coupled with the rootzone soil moisture using an integrated approach. Consequently, this may explain why the all pairwise comparison showed the trends and magnitudes of FLEX-Topo and WaPOR estimates not to be significantly (*p-value* > 0.05) different (in both dry miombo woodland and wet miombo woodland) in the dormant phenophase in the dry season (Table A4 in the supplementary data). Therefore, the integration of soil moisture in evaporation simulation and the accuracy of the soil moisture product(s) used in coupling the transpiration with rootzone is likely to affect the magnitudes of satellite-based transpiration estimates.

3.82 Optimisation of the rooting depth

1320 Optimising rooting depth than the use of the standard one metre has been shown to increase transpiration of trees in landscapes with a dry season (Kleidon and Heimann, 1998). Modifying rooting depth can improve energy flux simulations at both field scale and regional scale (Liu *et al.,* 2020). Rooting depth has been shown to be sensitive to local soil water profiles determined by precipitation infiltration depth and ground water table depth from below (Fan *et al.,* 2017). Wang-

1325 Erlandsson *et al.* (2016) showed that accurate root zone storage estimates "improved evaporation simulation overall, and in particular during the least evaporating months in sub-humid to humid regions with moderate to high seasonality". Their study demonstrated that several forest types have developed rootzone storage mechanisms that helps buffering dry season conditions. The experiment by Li *et al.* (2021) showed that after afforestation the root zone storage between 1 to

1330 18m depth decreased by 1200m. This result pointed to the role of deep rooting of trees on root zone storage. However, Li *et al.* (2021) also showed that "growing deep roots has opposing roles: it promotes transpiration when there is sufficient available water in deep soil, but inhibits transpiration via decreasing stomatal conductance when available water in deep soil is exhausted". As earlier stated miombo species are deep rooting, beyond 5 metres, while the soil moisture in the

1335 miombo woodland increases with depth (i.e., Chidumayo, 2001; Savory, 1963). Therefore, one of the potential causes of the observed differences in satellite-based evaporation estimates could be the rooting depth used in the simulation of evaporation. The satellite-based evaporation estimates used in this study are likely not to have optimised rooting depth for the miombo woodland as there are no studies in public domain that have investigated the optimum rooting depth for effective

1340 simulation of transpiration of the miombo woodland. Various water cycle components in several regions indicates that plants have adapted to local climatic conditions such as variations in precipitation, temperature, active photosynthetic radiation and abiotic conditions such as soil type and soil water supply at the ecosystem scale (Tian *et al.,* 2018). Therefore, global scale root storage estimates and optimisation (i.e., Wang-Erlandsson *et al.*, 2016) may not be able to effectively

1345 capture the climatic conditions at local and region scales. The none optimisation of the rooting depth for the miombo woodland may explain why satellite-based estimates, at point scale, appeared to underestimate evaporation of the miombo woodland in the dry season (Zimba *et al.,* 2023).

3.83 Differences in land cover products used for evaporation simulation

1350

Among many other contributing factors, the land cover product or proxies as a model input in satellite-based evaporation estimates may largely explain the observed differences in both temporal and spatial distribution of evaporation. Globally, Wang-Erlandsson *et al.* (2016) found that the root zone storage was dependent on the type of land cover. For instance, the MOD16 uses

1355 a global land-cover product (Gray *et al.*, 2019; Running *et al.*, 2019) which had shown to misclassify certain land cover types and showed low user accuracy in certain regions (i.e., Leroux *et al.,* 2014). The WaPOR uses the Copernicus land cover product, but adds the distinction between irrigated and rain-fed areas (FAO, 2018). For the vegetation fraction, the GLEAM uses the MODIS MOD44B product (Martens *et al.,* 2017; Miralles *et al.,* 2011). Other satellite-based evaporation

1360 estimates (i.e., SSEBop) use vegetation indices such as the NDVI as proxy for vegetation cover.

Different vegetation types have different phenology-water interactions (i.e., Lu *et al.,* 2006) which influence actual evaporation (Forster *et al.*, 2022; Snyder *et al.*, 2013; Schwartz, 2013). Evaporation of the miombo woodland in the dry season mainly occurs through plant transpiration (as demonstrated by Tian *et al.,* (2018)), which is dependent on the landcover type,

1365 and is driven by root zone water availability and climate variables such as net radiation, air pressure, wind speed, air temperature and relative humidity (Wang-Erlandsson *et al.*, 2016; Gates & Hanks, 2015; Stancalie & Nert, 2012; Allen *et al.,* 1998). The link between the above mentioned drivers and the plant transpiration includes the rooting depth, stomata conductance thresholds and surface roughness which are vegetation type and plant species dependent (i.e., Urban *et al.,* 2017;

1370 Wehr *et al.,* 2017; Gates & Hanks, 2015; Tuzet, 2011). Therefore, dissimilarities in the land cover products, and including proxies (i.e., NDVI) and their associated accuracy limitations, possibly reflect in differences in the spatial-temporal distribution of the satellite-based actual evaporation estimates.

1375 **3.84   Satellite-based rainfall products and rainfall interception**

The differences observed in satellite-based evaporation estimates during the green-up, maturity/peak and the senescence/green-down phenophases may be more related to differences in quality of satellite-based precipitation products used and the ability of the models to effectively account for rainfall interception. Studies have shown that satellite precipitation products are

1380 geographically biased towards either underestimation or overestimation (i.e., Macharia *et al.,* 2022; Asadullah *et al.*, 2008; Dinku *et al.,* 2007). In the case of Africa no single precipitation product has been found to perform better than other precipitation products across landscapes and southern Africa in particular (i.e., Macharia *et al.,* 2022). The precipitation products, with different spatial resolutions and accuracy levels, used in the satellite-based evaporation estimates could

1385 explain the differences in the spatial-temporal distribution of satellite-based evaporation estimates in during the rainy season. For instance, FLEX-Topo used the Climate Hazards Group Infra-Red Precipitation with Station data (CHIRPS) (Funk *et al.,* 2015), GLEAM uses Multi-Source Weighted-Ensemble Precipitation (MSWEP) (Bai and Liu, 2018) which are estimated with different algorithms, inputs and spatial resolutions. Interception is a function of vegetation cover,

1390 LAI and precipitation (FAO, 2018; Gerrits, 2010). For instance, the LAI influences canopy interception, through fall and forest floor interception (FAO, 2018; Gerrits, 2010). Field observations showed that wet miombo woodland canopies intercepted up to 18-20 percent of rainfall annually (i.e., Alexandre, 1977). As earlier mentioned above, the accuracy of the vegetation cover product influences the classification of the various vegetation types. Therefore,

1395 differences in the quality and accuracy of land cover products and even proxies such as the NDVI used for modelling interception is likely to result in differences in the spatial-temporal distribution of actual evaporation estimates among satellite-based evaporation estimates with have interception modules (i.e., FLEX-Topo, GLEAM, MOD16 and WaPOR). The differences in the algorithms and inputs in estimating the rainfall interception may also contribute to these differences in

1400 satellite-based evaporation estimates in the phenophases in the rainy season. Differences in the quality of the rainfall products used in the satellite-based evaporation estimates consequently influences the rainfall interception estimates.

4   Conclusions and recommendations

1405 The study sought to find out the extent to which satellite-based evaporation estimates were similar to each other across the different phenophases of the miombo woodland. The study also sought to establish the potential underlying factor(s) for the discrepancies. Furthermore, the study

compared the satellite-based actual evaporation estimates to the annual general water balance-based actual evaporation estimates at basin scale. This helped to establish whether the heterogeneity in the landscape at the Luangwa Basin scale would give a different result to that observed at point scale in the wet miombo woodland. The following were the conclusions:

All satellite-based evaporation estimates strongly correlated with the changes in phenology (i.e., proxied by the NDVI) in the green-up and senescence/green-down phenophases, but showed relatively weaker correlations in the dormant and maturity/peak phenophases. Furthermore, weaker correlations and high coefficients of variation among satellite-based evaporation estimates were observed in the dormant phenophase in the dry season. Therefore, the observed differences in satellite-based evaporation estimates in the dry season appears to be due to limited understanding and inadequate representation of the phenology-water interactions, that are influenced by the adapted physiological attributes such as the deep rooting and vegetation water storage of the miombo species. It is therefore, possible that the underestimations observed when satellite-based evaporation estimates are compared to the water-balance based evaporation estimates are not only as a result of the inadequate representation of the phenology-water interactions of the miombo species but also other vegetation types such as the mopane species that are also a part of the Luangwa basin vegetation cover. Consequently, field observations of evaporation across the different phenophases and strata of the miombo woodland are needed in order to have a comprehensive overview of the characteristics of the actual evaporation of the ecosystem. This information can be used to help improve satellite-based evaporation assessments in the Luangwa Basin and the miombo region as whole.

Based on the unique phenology such as the increase in LAI before commencement of seasonal rainfall and the adapted deep rooting; direct integration of the soil moisture and optimising the rooting depth for coupling with canopy transpiration is likely to improve estimates of transpiration of the miombo woodland in the dry season.

Author contribution

Conceptualization, H.Z.; formal analysis, H.Z., P.H; resources, H.S.; supervision, M.C.-G. and B.K.; writing—original draft, H.Z.; writing—review and editing, M.C.-G., B.K., H.S., P.H., I.N., and N.V. All authors have read and agree to the published version of the manuscript.

Funding

This study was conducted with the financial support of the Dutch Research Council (NWO) under the project number W 07.303.102.

Acknowledgements

This study is part of the ZAMSECUR Project, which focuses on observing and understanding the remote water resources for enhancing water, food and energy security in Lower Zambezi Basin We wish to thank the Water Resources Management Authority (WARMA) in Zambia for the field discharge data used in this study.

Conflict of interest:

At least one of the (co-)authors is a member of the editorial board of Hydrology and Earth System Sciences.

References

1455 Abatzoglou, J. T., Dobrowski, S. Z., Parks, S. A., & Hegewisch, K. C.: TerraClimate, a high-resolution global dataset of monthly climate and climatic water balance from 1958-2015. *Scientific Data*, *5*, 1–12. doi:10.1038/sdata.2017.191, 2018.

Abrams, M., & Crippen, R.: ASTER Global DEM (Digital Elevation Mode) - Quick Guide for V3. *California Institute of Technology*, *3*(July), 10, 2019.

1460 Allen R., G., Pereira L. S., Raes D, Smith M.: Crop evapotranspiration - guidelines for computing crop water requirements. FAO irrigation and drainage paper 56, Rome, Italy http://www.fao.org/docrep/X0490E/X0490E00.htm, 1998.

Alexandre, J.: Le bilan de l'eau dans le miombo (forêt claire tropicale). Bulletein de la Société Géographie du Liège 13, 107-126, 1977.

1465

Asadullah, A., McIntyre, N., & Kigobe, M.: Evaluation of five satellite products for estimation of rainfall over Uganda. *Hydrological Sciences Journal*, *53*(6), 1137–1150. doi:10.1623/hysj.53.6.1137, 2008.

Bai, P. and Liu, X.: Intercomparison and evaluation of three global high-resolution
1470 evapotranspiration products across China, J. Hydrol., 566, 743–755, https://doi.org/10.1016/j.jhydrol.2018.09.065, 2018.

Beilfuss, R.: A Risky Climate for Southern African Hydro ASSESSING HYDROLOGICAL RISKS AND A Risky Climate for Southern African Hydro, (September).
1475 doi:10.13140/RG.2.2.30193.48486, 2012.

Biggs, T., Petropoulos, G. P., Velpuri, N. M., Marshall, M., Glenn, E. P., Nagler, P., & Messina, A.: Remote sensing of actual evapotranspiration from croplands. Remote Sensing Handbook: Remote Sensing of Water Resources, Disasters, and Urban Studies, 59-99, 2015.

1480 Bogawski, P., Bednorz, E.: Comparison and Validation of Selected Evapotranspiration Models for Conditions in Poland (Central Europe). *Water Resour Manage* **28**, 5021–5038. https://doi.org/10.1007/s11269-014-0787-8, 2014.

Bonnesoeur, V., Locatelli, B., Guariguata, M. R., Ochoa-Tocachi, B. F., Vanacker, V., Mao, Z.,
1485 … Mathez-Stiefel, S. L.: Impacts of forests and forestation on hydrological services in the Andes: A systematic review. *Forest Ecology and Management*, *433*(June 2018), 569–584. doi:10.1016/j.foreco.2018.11.033, 2019.

Brust, C., Kimball, J. S., Maneta, M. P., Jencso, K., He, M., & Reichle, R. H.: Using SMAP Level-4 soil moisture to constrain MOD16 evapotranspiration over the contiguous USA.
1490 *Remote Sensing of Environment*, *255*(January), 112277. doi:10.1016/j.rse.2020.112277, 2021.

Buchhorn, M.; Smets, B.; Bertels, L.; De Roo, B.; Lesiv, M.; Tsendbazar, N.E., Linlin, L., Tarko, A.: *Copernicus Global Land Service: Land Cover 100m: Version 3 Globe 2015-2019: Product User Manual*. Zenodo, Geneve, Switzerland.
1495 https://doi.org/10.5281/zenodo.3938963, 2020.

Campbell, B., Frost, P., & Bryon, N.: miombo woodlands and their use: overview and key issues.In "The Miombo in Transition: Woodlands and Welfare in Africa. Ed: B. Campbell (Bogor, Indonesia: Center for International Forestry Research) p 1–6, 1996.

Chen, Y., Xia, J., Liang, S., Feng, J., Fisher, J. B., Li, X., … Yuan, W.: Comparison of satellite-based evapotranspiration models over terrestrial ecosystems in China. *Remote Sensing of Environment*, *140*, 279–293. doi:10.1016/j.rse.2013.08.045, 2014.

Chidumayo, E. N.: Climate and Phenology of Savanna Vegetation in Southern Africa. *Journal of Vegetation Science*, *12*(3), 347. doi: 10.2307/3236848, 2001.

Chidumayo, E, N., & Frost, P.: Population biology of miombo trees. In The miombo in transition: woodlands and welfare in Africa, Campbell, B. (ed.). Bogor (Indonesia): CIFOR, ISBN 979-8764-07-2, 1996.

Chidumayo, E. N.: Phenology and nutrition of miombo woodland trees in Zambia. *Trees*, *9*(2), 67–72. doi:10.1007/BF00202124, 1994.

Cleland, E. E., Chuine, I., Menzel, A., Mooney, H. A., & Schwartz, M. D.: Shifting plant phenology in response to global change. *Trends in Ecology and Evolution*, *22*(7), 357–365. doi:10.1016/j.tree.2007.04.003, 2007.

Dinku, T., Ceccato, P., Grover-Kopec, E., Lemma, M., Connor, S. J., & Ropelewski, C. F.: Validation of satellite rainfall products over East Africa's complex topography. *International Journal of Remote Sensing*, *28*(7), 1503–1526. doi:10.1080/01431160600954688, 2007.

Ernst, W. and Walker, B.H.: Studies on the hydrature of trees in miombo woodland in South Central Africa. Journal of Ecology 61, 667-673, 1973.

FAO.: *WaPOR Database Methodology: Level 1 Data*. *Remote Sensing for Water Productivity Technical Report: Methodology Series*. Retrieved from http://www.fao.org/fileadmin/user_upload/faoweb/RS-WP/pdf_files/Web_WaPOR-beta_Methodology_document_Level1.pdf, last accessed: 20 June, 2022, 2018

Forrest, J., Inouye, D. W., & Thomson, J. D.: Flowering phenology in subalpine meadows: Does climate variation influence community co-flowering patterns? *Ecology*, *91*(2), 431–440. doi:10.1890/09-0099.1, 2010.

Forrest, J., & Miller-Rushing, A. J.: Toward a synthetic understanding of the role of phenology in ecology and evolution. *Philosophical Transactions of the Royal Society B: Biological Sciences*, *365*(1555), 3101–3112. doi:10.1098/rstb.2010.0145, 2010.

Forster, M. A., Kim, T. D. H., Kunz, S., Abuseif, M., Chulliparambil, V. R., Srichandra, J., & Michael, R. N.: Phenology and canopy conductance limit the accuracy of 20 evapotranspiration models in predicting transpiration. *Agricultural and Forest Meteorology*, *315*(December 2021), 108824. doi:10.1016/j.agrformet.2022.108824, 2022.

Friedl, M., Gray, J., Sulla-Menashe, D.: MCD12Q2 MODIS/Terra+Aqua Land Cover
    Dynamics Yearly L3 Global 500m SIN Grid V006 [Data set]. NASA EOSDIS Land
    Processes DAAC. Accessed 2023-03-30 from
1540   https://doi.org/10.5067/MODIS/MCD12Q2.006, 2019.

Frost, P.: *The Ecology of Miombo Woodlands*. (B. Campbell, Ed.), *The Miombo in Transition:
    Woodlands and Welfare in Africa*. Bogor, Indonesia: Center for International Forestry
    Research. Retrieved from
1545   http://books.google.com/books?hl=nl&lr=&id=rpildJJVdU4C&pgis=1, last accessed: 20
    June 2022, 1996.

Fuller, D. O.: Canopy phenology of some mopane and miombo woodlands in eastern Zambia.
    Global Ecology and Biogeography, *8*(3–4), 199–209. doi:10.1046/j.1365-
    2699.1999.00130.x, 1999.

1550 Fuller, D. O., & Prince, S. D.: Rainfall and foliar dynamics in tropical southern Africa: Potential
    impacts of global climatic change on Savanna vegetation. *Climatic Change*, *33*(1), 69–96.
    doi:10.1007/BF00140514, 1996.

Funk, C., Peterson, P., Landsfeld, M., Pedreros, D., Verdin, J., Shukla, S., Husak, G., Rowland,
    J., Harrison, L., Hoell, A., & Michaelsen, J.: The climate hazards infrared precipitation with
1555   stations - A new environmental record for monitoring extremes. *Scientific Data*, *2*, 1–21.
    doi: 10.1038/sdata.2015.66, 2015.

García, L., Rodríguez, J. D., Wijnen, M., & Pakulski, I.: *Earth Observation for Water Resources
    Management: Current Use and Future Opportunities for the Water Sector*. Washington, DC
    20433: Washington, DC: World Bank. doi:10.1596/978-1-4648-0475-5, 2016.

1560 Gates, D. M., & Hanks, R. J.: Plant factors affecting evapotranspiration. *Irrigation of
    Agricultural Lands*, *11*, 506–521. doi:10.2134/agronmonogr11.c28, 2015.

Gerrits, A.M.J.: The role of interception in the hydrological cycle. Dissertation Delft
    University of Technology. ISBN: 978-90-6562-248-8
1565   http://resolver.tudelft.nl/uuid:7dd2523b-2169-4e7e-992c-365d2294d02e, 2010.

Gokmen, M., Vekerdy, Z., Verhoef, A., Verhoef, W., Batelaan, O., & van der Tol, C.:
    Integration of soil moisture in SEBS for improving evapotranspiration estimation under
    water stress conditions. *Remote Sensing of Environment*, *121*, 261–274.
1570   doi:10.1016/j.rse.2012.02.003, 2012.

Gray, J., Sulla-Menashe, D., & Friedl, M. A: MODIS Land Cover Dynamics (MCD12Q2)
    Product. *User Guide Collection 6*, *6*, 8. Retrieved from https://modis-
    land.gsfc.nasa.gov/pdf/MCD12Q2_Collection6_UserGuide.pdf, last accessed: 20 June
    2022, 2019.

1575 Guan, K., Eric F. Wood, D. Medvigy, John. Kimball, Ming. Pan, K.K. Caylor, J. Sheffield,
    Xiangtao. Xu, and O.M. Jones.: Terrestrial hydrological controls on land surface phenology
    of African savannas and woodlands. *Journal of Geophysical Research: Biogeosciences*,
    119(8), 1652–1669. doi:10.1002/2013JG002572, 2014, 2014.

Han, J., Zhao, Y., Wang, J., Zhang, B., Zhu, Y., Jiang, S., & Wang, L.: Effects of different land use types on potential evapotranspiration in the Beijing-Tianjin-Hebei region, North China. *Journal of Geographical Sciences*, *29*(6), 922–934. doi:10.1007/s11442-019-1637-7, 2019.

Helsel, D. R., R. M. Hirsch, K.R. Ryberg, S.A. Archfield, and E.J. Gilroy.: "Statistical Methods in Water Resources Techniques and Methods 4 – A3." *USGS Techniques and Methods*, 2020.

Hersbach, H., Bell, B., Berrisford, P., Hirahara, S., Horányi, A., Muñoz-Sabater, J., Nicolas, J., Peubey, C., Radu, R., Schepers, D., Simmons, A., Soci, C., Abdalla, S., Abellan, X., Balsamo, G., Bechtold, P., Biavati, G., Bidlot, J., Bonavita, M., De Chiara, G., Dahlgren, P., Dee, D., Diamantakis, M., Dragani, R., Flemming, J., Forbes, R., Fuentes, M., Geer, A., Haimberger, L., Healy, S., Hogan, R.J., Hólm, E., Janisková, M., Keeley, S., Laloyaux, P., Lopez, P., Lupu, C., Radnoti, G., de Rosnay, P., Rozum, I., Vamborg, F., Villaume, S., Thépaut, J-N.: Complete ERA5 from 1979: Fifth generation of ECMWF atmospheric reanalyses of the global climate. Copernicus Climate Change Service (C3S) Data Store (CDS). (Accessed on 06-06-2022), 2017.

Hulsman, P., Hrachowitz, M., & Savenije, H. H. G.: Improving the Representation of Long-Term Storage Variations With Conceptual Hydrological Models in Data-Scarce Regions. *Water Resources Research*, *57*(4). doi:10.1029/2020WR028837, 2021.

Hulsman, P., Winsemius, H. C., Michailovsky, C. I., Savenije, H. H. G., & Hrachowitz, M.: Using altimetry observations combined with GRACE to select parameter sets of a hydrological model in a data-scarce region. *Hydrology and Earth System Sciences*, *24*(6), 3331–3359. doi:10.5194/hess-24-3331-2020, 2020.

Jeffers, J. N., & Boaler, S. B., 1966. Ecology of a miombo site. Lupa North Forest Reserve, Tanzania. I. Weather and plant growth , 1962–64'. *Ecology, 54*, 447–463.

Jiménez, C., Prigent, C., Mueller, B., Seneviratne, S. I., McCabe, M. F., Wood, E. F., … Wang, K.: Global intercomparison of 12 land surface heat flux estimates. *Journal of Geophysical Research Atmospheres*, *116*(2), 1–27. doi:10.1029/2010JD014545, 2011.

Jiménez, C., Prigent, C., & Aires, F.: Toward an estimation of global land surface heat fluxes from multisatellite observations. *Journal of Geophysical Research Atmospheres*, *114*(6), 1–22. doi:10.1029/2008JD011392, 2009.

Kleine, L., Tetzlaff, D., Smith, A., Dubbert, M., & Soulsby, C.: Modelling ecohydrological feedbacks in forest and grassland plots under a prolonged drought anomaly in Central Europe 2018–2020. *Hydrological Processes*, *35*(8). doi:10.1002/hyp.14325, 2021.

Kramer, K., Leinonen, I., & Loustau, D.: The importance of phenology for the evaluation of impact of climate change on growth of boreal, temperate and Mediterranean forests ecosystems: An overview. *International Journal of Biometeorology*. doi:10.1007/s004840000066, 2000.

Leroux, L., Jolivot,A., Bégué,A., Lo Seen,D., and Zoungrana, B.: "How Reliable Is the MODIS Land Cover Product for Crop Mapping Sub-Saharan Agricultural Landscapes?" *Remote Sensing* 6(9):8541–64. doi: 10.3390/rs6098541, 2014.

Li, H., Ma, X., Lu, Y., Ren, R., Cui, B., & Si, B.: Growing deep roots has opposing impacts on the transpiration of apple trees planted in subhumid loess region. Agricultural Water Management, 258(June), 107207. doi: 10.1016/j.agwat.2021.107207, 2021.

Liu. M, & Hu. D.: Response of Wetland Evapotranspiration to Land Use/Cover Change and Climate Change in Liaohe River Delta, China. *Water*; 11(5):955. https://doi.org/10.3390/w11050955, 2019.

Liu, Wenbin, Lei Wang, Jing Zhou, Yanzhong Li, Fubao Sun, Guobin Fu, Xiuping Li, and Yan Fang Sang.: "A Worldwide Evaluation of Basin-Scale Evapotranspiration Estimates against the Water Balance Method." *Journal of Hydrology* 538: 82–95. https://doi.org/10.1016/j.jhydrol.2016.04.006, 2016.

Lu, P., Yu, Q., Liu, J., & Lee, X.: Advance of tree-flowering dates in response to urban climate change. *Agricultural and Forest Meteorology*, *138*(1–4), 120–131. doi:10.1016/j.agrformet.2006.04.002, 2006.

Macharia, D., Fankhauser, K., Selker, J. S., Neff, J. C., & Thomas, E. A.: Validation and Intercomparison of Satellite-Based Rainfall Products over Africa with TAHMO In Situ Rainfall Observations. *Journal of Hydrometeorology*, *23*(7), 1131–1154. doi:10.1175/JHM-D-21-0161.1, 2022.

Makapela, L.: *Review and use of earth observations and remote sensing in water resource management in South Africa : report to the Water Research Commission*, 2015.

Marchesini, V. A., Fernández, R. J., Reynolds, J. F., Sobrino, J. A., & Di Bella, C. M.: Changes in evapotranspiration and phenology as consequences of shrub removal in dry forests of central Argentina. *Ecohydrology*, *8*(7), 1304–1311. doi:10.1002/eco.1583, 2015.

Martens, B., Miralles, D. G., Lievens, H., Van Der Schalie, R., De Jeu, R. A. M., Fernández-Prieto, D., … Verhoest, N. E. C.: GLEAM v3: Satellite-based land evaporation and root-zone soil moisture. *Geoscientific Model Development*, *10*(5), 1903–1925. doi:10.5194/gmd-10-1903-2017, 2017.

Martins, J. P., Trigo, I., & Freitas, S. C. E.: Copernicus Global Land Operations "Vegetation and Energy" "CGLOPS-1". *Copernicus Global Land Operations*, 1–93. doi:10.5281/zenodo.3938963.PU, 2020.

Miralles, D. G., Brutsaert, W., Dolman, A. J., & Gash, J. H.: On the Use of the Term "Evapotranspiration". *Water Resources Research*, *56*(11). doi:10.1029/2020WR028055, 2020.

Miralles, D. G., De Jeu, R. A. M., Gash, J. H., Holmes, T. R. H., & Dolman, A. J.: Magnitude and variability of land evaporation and its components at the global scale. *Hydrology and Earth System Sciences*, *15*(3), 967–981. doi:10.5194/hess-15-967-2011, 2011.

Mittermeier, R. A., Mittermeier, C. G., Brooks, T. M., Pilgrim, J. D., Konstant, W. R., Da Fonseca, G. A. B., & Kormos, C.: Wilderness and biodiversity conservation. *Proceedings of the National Academy of Sciences of the United States of America*, *100*(18), 10309–10313. doi:10.1073/pnas.1732458100, 2003.

Mu, Q., Zhao, M., and Running, W.S.: Improvements to a MODIS Global Terrestrial Evapotranspiration Algorithm. *Remote Sensing of Environment* 115 (8): 1781–1800. https://doi.org/10.1016/j.rse.2011.02.019, 2011.

1665

Mu, Q., Heinsch, F. A., Zhao, M., & Running, S. W.: Development of a global evapotranspiration algorithm based on MODIS and global meteorology data. *Remote Sensing of Environment*, *111*(4), 519–536. doi:10.1016/j.rse.2007.04.015, 2007.

Myneni, R., Knyazikhin, Y., and Park, T.: MCD15A2H MODIS/TerraCAqua Leaf Area
1670   Index/FPAR 8-day L4 Global 500m SIN Grid V06, NASA EOSDIS Land Processes DAAC [data set], https://doi.org/10.5067/MODIS/MCD15A2H.061, 2021.

Myneni, R., & Park, Y. K.: *MCD15A2H MODIS/Terra+Aqua Leaf Area Index/FPAR 8-day L4 Global 500m SIN Grid V006.* NASA EOSDIS Land Processes DAAC. Retrieved from
1675   https://doi.org/10.5067/MODIS/MCD15A2H.006, (last accessed: 20 January, 2023) 2015.

Niu,S., Fu,Y., Gu,L., and and Luo, Y.: Temperature Sensitivity of Canopy Photosynthesis Phenology in Northern Ecosystems. Pp. 503–19 in *Phenology: An Integrative Environmental Science*, edited by M. D. Schwartz., 2013.

1680   Nord, E. A., & Lynch, J. P.: Plant phenology: A critical controller of soil resource acquisition. *Journal of Experimental Botany*, *60*(7), 1927–1937. doi:10.1093/jxb/erp018, 2009.

Novick, K. A., Ficklin, D. L., Stoy, P. C., Williams, C. A., Bohrer, G., Oishi, A. C., Papuga, S. A., Blanken, P. D., Noormets, A., Sulman, B. N., Scott, R. L., Wang, L., & Phillips, R. P.: The increasing importance of atmospheric demand for ecosystem water and carbon fluxes.
1685   *Nature Climate Change*, *6*(11), 1023–1027. doi:10.1038/nclimate3114, 2016.

ORNL DAAC., 2018. MODIS and VIIRS Land Products Global Subsetting and Visualization Tool, Subset obtained for MCD12Q2 product at [-12:76252], [32.48406], time period: [31-12-2020] to [31-12-2021], and subset size: [4]_[4] km,ORNL DAAC, Oak Ridge, Tennessee, USA [data set],https://doi.org/10.3334/ORNLDAAC/1379.

1690

Pelletier, J., Paquette, A., Mbindo, K., Zimba, N., Siampale, A., Chendauka, B., Siangulube, F., & Roberts, J. W.: Carbon sink despite large deforestation in African tropical dry forests (miombo woodlands). *Environmental Research Letters*, *13*(9). doi:10.1088/1748-9326/aadc9a, 2018.

1695   Pereira, C. C., Boaventura, M. G., Cornelissen, T., Nunes, Y. R. F., & de Castro, G. C.: What triggers phenological events in plants under seasonal environments? A study with phylogenetically related plant species in sympatry. *Brazilian Journal of Biology*, *84*(March). doi:10.1590/1519-6984.257969, 2022.

Roberts, J. M.: *The role of forests in the hydrological cycle. Forests and forest plants* (Vol. III).
1700   Retrieved from https://www.eolss.net/sample-chapters/c10/E5-03-04-02.pdf, last accessed: 20 June, 2022, (not dated).

Running, Steven W, Qiaozhen Mu, Maosheng Zhao, A. M.:. User ' s Guide MODIS Global Terrestrial Evapotranspiration (ET) Product NASA Earth Observing System MODIS Land Algorithm (For Collection 6) (last accessed: 20 January, 2023), 2019.

Ryan, C. M., Pritchard, R., McNicol, I., Owen, M., Fisher, J. A., & Lehmann, C.: Ecosystem services from southern African woodlands and their future under global change. *Philosophical Transactions of the Royal Society B: Biological Sciences*, *371*(1703). doi:10.1098/rstb.2015.0312, 2016.

Saha, S., Moorthi, S., Wu, X., Wang, J., & Coauthors.: The NCEP Climate Forecast System Version 2. *Journal of Climate, 27*, 2185–2208. doi:10.1175/JCLI-D-12-00823.1, 2014.

Saha, S., Moorthi, S., Pan, H., Wu,, X., Wang, J., & Coauthors.: The NCEP Climate Forecast System Reanalysis. *Bulletin of the American Meteorological Society, 91*, 1015–1057. doi:10.1175/2010BAMS3001.1, 2010.

Santin-Janin, H., Garel, M., Chapuis, J. L., & Pontier, D.: Assessing the performance of NDVI as a proxy for plant biomass using non-linear models: A case study on the kerguelen archipelago. *Polar Biology*, *32*(6), 861–871. doi:10.1007/s00300-009-0586-5, 2009.

Savenije, H. H.G.: HESS opinions 'topography driven conceptual modelling (FLEX-Topo)'. *Hydrology and Earth System Sciences*, *14*(12), 2681–2692. doi:10.5194/hess-14-2681-2010, 2010.

Savenije, Hubert H.G.: The importance of interception and why we should delete the term evapotranspiration from our vocabulary. *Hydrological Processes*, *18*(8), 1507–1511. doi:10.1002/hyp.5563, 2004.

Savory, B. M.: Site quality and tree root morphology in Northern Rhodesia, Rhodes. J. Agricult. Res., 1, 55–64, 1963.

Schwartz, M. D.: *Phenology: An Integrative Environmental Science*. (M. D. Schwartz, Ed.), *Phenology: An Integrative Environmental Science* (Second Edi). Dordrecht: Springer Netherlands. doi:10.1007/978-94-007-6925-0_27, 2013.

Senay, G. B., Bohms, S., Singh, R. K., Gowda, P. H., Velpuri, N. M., Alemu, H., & Verdin, J. P.: Operational Evapotranspiration Mapping Using Remote Sensing and Weather Datasets: A New Parameterization for the SSEB Approach. *Journal of the American Water Resources Association*, *49*(3), 577–591. doi:10.1111/jawr.12057, 2013.

Shahidan, M. F., Salleh, E., & Mustafa, K. M. S.: Effects of tree canopies on solar radiation filtration in a tropical microclimatic environment. *Sun, Wind and Architecture - The Proceedings of the 24th International Conference on Passive and Low Energy Architecture, PLEA 2007*, (November), 400–406, 2007.

Sheil, D.: Forests, atmospheric water and an uncertain future: the new biology of the global water cycle. *Forest Ecosystems*, *5*(1). doi:10.1186/s40663-018-0138-y, 2018.

Snyder, R. L., & Spano, D.: Phenology and Evapotranspiration. In Mark D. Schwartz (Ed.), *Phenology: An Integrative Environmental Science* (Second, pp. 521–528). Milwaukee, 2013.

Stancalie, G., & Nert, A.: Possibilities of Deriving Crop Evapotranspiration from Satellite Data with the Integration with Other Sources of Information. *Evapotranspiration - Remote Sensing and Modeling*, (January). doi:10.5772/23635, 2012.

Stökli, R., T. Rutishauser, I. Baker, M. A. Liniger, and A. S. Denning.: "A Global Reanalysis of Vegetation Phenology." *Journal of Geophysical Research: Biogeosciences* 116 (3): 1–19. https://doi.org/10.1029/2010JG001545, 2011.

Tian, F., Wigneron, J. P., Ciais, P., Chave, J., Ogée, J., Peñuelas, J., … Fensholt, R.: Coupling of ecosystem-scale plant water storage and leaf phenology observed by satellite. *Nature Ecology and Evolution*, *2*(9), 1428–1435. doi:10.1038/s41559-018-0630-3, 2018.

Tuzet, A. J.: Stomatal Conductance, Photosynthesis, and Transpiration, Modeling. In J. Gliński, J., Horabik, J., Lipiec (Ed.), *Encyclopedia of Agrophysics. Encyclopedia of Earth Sciences Series* (pp. 855–858). Dordrecht. doi:10.1007/978-90-481-3585-1_213, 2011.

Urban, J., Ingwers, M. W., McGuire, M. A., & Teskey, R. O.: Increase in leaf temperature opens stomata and decouples net photosynthesis from stomatal conductance in Pinus taeda and Populus deltoides x nigra. *Journal of Experimental Botany*, *68*(7), 1757–1767. doi:10.1093/jxb/erx052, 2017.

Van Der Ent, R. J., Wang-Erlandsson, L., Keys, P. W., & Savenije, H. H. G.: Contrasting roles of interception and transpiration in the hydrological cycle – Part 2: Moisture recycling. *Earth System Dynamics*, *5*(2), 471–489. doi:10.5194/esd-5-471-2014, 2014.

Van Der Ent, Rudi J., Savenije, H. H. G., Schaefli, B., & Steele-Dunne, S. C.: Origin and fate of atmospheric moisture over continents. *Water Resources Research*, *46*(9), 1–12. doi:10.1029/2010WR009127, 2010

Vermote, E., Wolfe, R.: MOD09GA MODIS/Terra Surface Reflectance Daily L2G Global 1kmand 500m SIN Grid V006 [Data set]. NASA EOSDIS Land Processes DAAC. Accessed 2022-10-01 from https://doi.org/10.5067/MODIS/MOD09GA.006, 2015.

Vinya, R., Malhi, Y., Brown, N. D., Fisher, J. B., Brodribb, T., & Aragão, L. E.: Seasonal changes in plant–water relations influence trends of leaf display in Miombo woodlands: evidence of water conservative strategies. *Tree Physiology, 39*, 04–112. doi:doi:10.1093/treephys/tpy062, 2018.

Wang, S., Fu, B. J., Gao, G. Y., Yao, X. L., & Zhou, J.: Soil moisture and evapotranspiration of different land cover types in the Loess Plateau, China. *Hydrology and Earth System Sciences*, *16*(8), 2883–2892. doi: 10.5194/hess-16-2883-2012, 2012.

Wang-Erlandsson, L., Bastiaanssen, W. G. M., Gao, H., Jägermeyr, J., Senay, G. B., Van Dijk, A. I. J. M., … Savenije, H. H. G.: Global root zone storage capacity from satellite-based evaporation. *Hydrology and Earth System Sciences*, *20*(4), 1459–1481. doi:10.5194/hess-20-1459-2016, 2016.

WARMA.: Catchments for Zambia. Retrieved 9 February 2022, from http://www.warma.org.zm/catchments-zambia/luangwa-catchment-2/, 2022.

Weerasinghe, I., Bastiaanssen, W., Mul, M., Jia, L., & Van Griensven, A.: Can we trust remote sensing evapotranspiration products over Africa. *Hydrology and Earth System Sciences*, *24*(3), 1565–1586. doi:10.5194/hess-24-1565-2020, 2020.

1785 Wehr, R., Commane, R., Munger, J. W., Barry Mcmanus, J., Nelson, D. D., Zahniser, M. S., … Wofsy, S. C.: Dynamics of canopy stomatal conductance, transpiration, and evaporation in a temperate deciduous forest, validated by carbonyl sulfide uptake. *Biogeosciences*, *14*(2), 389–401. doi:10.5194/bg-14-389-2017, 2017.

White, F.: *The Vegetation of Africa; a descriptive memoir to accompany the*
1790 *UNESCO/AETFAT/UNSO vegetation map of Africa*. Paris: UNESCO. Retrieved from https://unesdoc.unesco.org/ark:/48223/pf0000058054 (Last accessed: 20 January, 2023), 1983.

World Bank.: "The Zambezi River Basin: A Multi-Sector Investment Opportunities Analysis – State of the Basin," World Bank Publications - Reports 2961, The World Bank Group.
1795 https://ideas.repec.org/p/wbk/wboper/2961.html, (Last accessed: 20 January 2023), 2010.

Zhang, K, Kimball, S. J., and Running, W.S.: A Review of Remote Sensing Based Actual Evapotranspiration Estimation. *Wiley Interdisciplinary Reviews: Water* 3 (6): 834–53. https://doi.org/10.1002/wat2.1168, 2016.

1800 Zhang, X., Friedl, M. A., Schaaf, C. B., Strahler, A. H., Hodges, J. C. F., Gao, F., Reed, B. C., & Huete, A.: Monitoring vegetation phenology using MODIS. *Remote Sensing of Environment*, *84*(3), 471–475. doi: 10.1016/S0034-4257(02)00135-9, 2003.

Zhao, M, Peng, C., Xiang, W., Deng, X., Tian, D., Zhou, X., Yu, G., He, H., and Zhao, Z.: "Plant Phenological Modeling and Its Application in Global Climate Change Research: Overview
1805 and Future Challenges." *Environmental Reviews* 21 (1): 1–14. https://doi.org/10.1139/er-2012-0036, 2013

Zimba, H., Coenders-Gerrits, M., Banda, K., Schilperoort, B., van de Giesen, N., Nyambe, I., and Savenije, H. H. G.: Phenophase-based comparison of field observations to satellite-based actual evaporation estimates of a natural woodland: miombo woodland, southern
1810 Africa, Hydrol. Earth Syst. Sci., 27, 1695–1722, https://doi.org/10.5194/hess-27-1695-2023, 2023.

Zimba, H., Coenders, M., Savenije, H. H. G., van de Giesen, N., & Hulsman, P.: ZAMSECUR Project Field Data Mpika, Zambia (Version 2) [Data set]. 4TU.ResearchData.
1815 https://doi.org/10.4121/19372352.V2, 2022.